Alexandria Engineering Journal (2016) 55, 875–905

Alexandria University

Alexandria Engineering Journal

www.elsevier.com/locate/aej
www.sciencedirect.com

ORIGINAL ARTICLE

MHD free convection flow of Eyring–Powell fluid from vertical surface in porous media with Hall/ionslip currents and ohmic dissipation

S. Abdul Gaffar [a,*], **V. Ramachandra Prasad** [b], **E. Keshava Reddy** [a]

[a] *Department of Mathematics, Jawaharlal Nehru Technological University Anantapur, Ananthapuramu 515002, India*
[b] *Department of Mathematics, Madanapalle Institute of Technology and Science, Madanapalle 517325, India*

Received 9 July 2015; revised 9 February 2016; accepted 20 February 2016
Available online 4 March 2016

KEYWORDS

Non-Newtonian Eyring–Powell model;
Viscous dissipation;
Non-Darcy model;
Hall currents;
Ionslip currents;
Forchheimer parameter

Abstract A mathematical study is presented to analyze the nonlinear, non-isothermal, magnetohydrodynamic (MHD) free convection boundary layer flow, heat and mass transfer of non-Newtonian Eyring–Powell fluid from a vertical surface in a non-Darcy, isotropic, homogenous porous medium, in the presence of Hall currents and ionslip currents. The governing nonlinear coupled partial differential equations for momentum conservation in the x, and z directions, heat and mass conservation, in the flow regime are transformed from an (x, y, z) coordinate system to a (ξ, η) coordinate system in terms of dimensionless x-direction velocity (f') and z-direction velocity (G), dimensionless temperature and concentration functions (θ and ϕ) under appropriate boundary conditions. Both Darcian and Forchheimer porous impedances are incorporated in both momentum equations. Computations are also provided for the variation of the x and z direction shear stress components and also heat and mass transfer rates. It is observed that with increasing ε, primary velocity, secondary velocity, heat and mass transfer rates are decreased whereas, the temperature, concentration and skin friction are increased. An increasing δ is found to increase primary and secondary velocities, skin friction, heat and mass transfer rates. But the temperature and concentration decrease. Increasing β_e and β_i are seen to increase primary velocity, skin friction, heat and mass transfer rates whereas secondary velocity, temperature and concentration are decreased. *Excellent correlation is achieved with a Nakamura tridiagonal finite difference scheme (**NTM**)*. The model finds applications in magnetic materials processing, MHD power generators and purification of crude oils.

1. Introduction

Analysis of non-Newtonian fluids has been the focus of several investigations during the past few decades because of its extensive engineering and industrial applications. Especially, flow

* Corresponding author.
E-mail address: abdulsgaffar0905@gmail.com (S. Abdul Gaffar).
Peer review under responsibility of Faculty of Engineering, Alexandria University.

http://dx.doi.org/10.1016/j.aej.2016.02.011

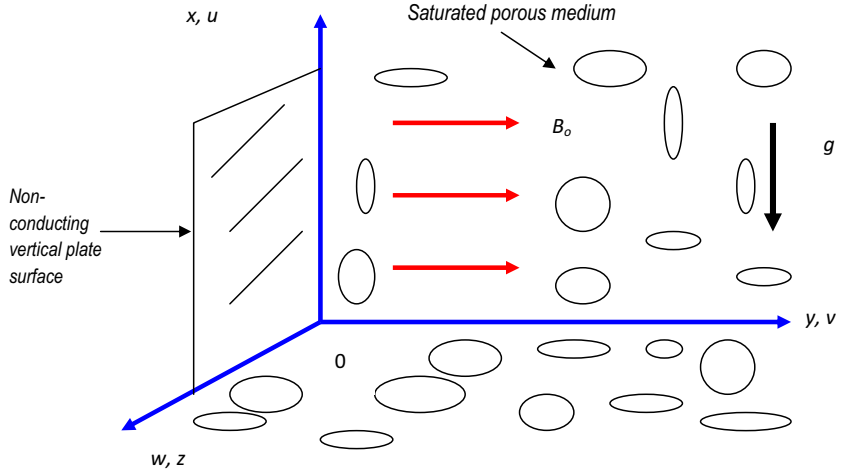

Figure 1 Physical model and coordinate system.

Table 1 Values of C_{fx}, Nu_x, and Sh_x for different ε, β_e, β_i and ξ ($\delta = 0.3$, $N_m = 0.5$, $Sc = 0.6$, $Gr = 1.0$, $Fs = Ec = Da = 0.1$, $N = 0.5$, $Pr = 7.0$).

ε	β_e	β_i	$\xi = 1.0$			$\xi = 2.0$			$\xi = 3.0$		
			C_{fx}	Nu_x	Sh_x	C_{fx}	Nu_x	Sh_x	C_{fx}	Nu_x	Sh_x
0.0	0.5	0.4	0.2752	0.5246	0.1713	0.0794	0.1140	0.1965	0.0363	0.2002	0.2170
0.18			0.2873	0.5216	0.1705	0.0855	0.1132	0.1950	0.0392	0.1935	0.2099
0.35			0.3007	0.5197	0.1683	0.0914	0.1127	0.1933	0.0420	0.1874	0.2042
0.52			0.3164	0.5193	0.1661	0.0972	0.1114	0.1931	0.0446	0.1850	0.2020
0.74			0.3333	0.5189	0.1654	0.1035	0.1105	0.1928	0.0477	0.1842	0.2014
1.0			0.3543	0.5162	0.1637	0.1105	0.1087	0.1922	0.0508	0.1822	0.1997
0.1	0.1	0.4	0.2806	0.5171	0.1658	0.0825	0.1088	0.1924	0.0375	0.1772	0.2003
	0.57		0.2818	0.5200	0.1645	0.0826	0.1090	0.1921	0.0375	0.1777	0.1994
	1.0		0.2826	0.5220	0.1635	0.0826	0.1091	0.1918	0.0376	0.1783	0.1988
	2.0		0.2836	0.5251	0.1623	0.0826	0.1095	0.1916	0.0377	0.1799	0.1983
	3.0		0.2840	0.5258	0.1618	0.0827	0.1098	0.1915	0.0378	0.1815	0.1980
	5.0		0.2843	0.5423	0.1614	0.0828	0.1102	0.1914	0.0380	0.1839	0.1979
0.1	0.5	0.0	0.2812	0.5185	0.1617	0.0826	0.1089	0.1915	0.0375	0.1776	0.1980
		1.0	0.2821	0.5208	0.1620	0.0826	0.1090	0.1916	0.0375	0.1780	0.1982
		3.0	0.2830	0.5230	0.1624	0.0826	0.1092	0.1916	0.0376	0.1786	0.1984
		5.0	0.2834	0.5241	0.1629	0.0826	0.1093	0.1918	0.0376	0.1793	0.1987
		8.0	0.2838	0.5248	0.1641	0.0827	0.1097	0.19120	0.0378	0.1810	0.1992
		12.0	0.2840	0.5254	0.1652	0.0827	0.1099	0.1922	0.0378	0.1825	0.1997

and heat transfer of non-Newtonian fluids play central role in food engineering, petroleum production, power engineering and in polymer solutions and in polymer melt in the plastic processing industries. In nature there are non-Newtonian fluids with different characteristics and consequently various constitutive equations of non-Newtonian fluids have been presented. The use of such constitutive equations leads to more complicated and highly nonlinear systems. The analytic/numerical solutions of such equations present exciting challenges to the mathematicians, physicists, numerical simulists and modelers. Significant attention has been directed at mathematical and numerical simulation of non-Newtonian fluids. Recent investigations have implemented, respectively the Casson model [1], tangent hyperbolic model [2], Eyring–Powell fluid model [3] and Jeffreys viscoelastic model [4].

Heat transfer in the presence of strong magnetic fields is important in various branches of magnetohydrodynamic power generation, nanotechnological processing, nuclear energy systems exploiting liquid metals and blood flow control. Nadeem et al. [5] investigated the MHD stagnation point flow of Carreau fluid toward a permeable shrinking sheet: Dual solutions. Akbar et al. [6] examined the dual solutions in MHD stagnation-point flow of Prandtl fluid impinging on shrinking sheet. Nadeem et al. [7] investigated the MHD three-dimensional Casson fluid flow past a porous linearly stretching sheet. Radiation effects on MHD stagnation point flow of nanofluid toward a stretching surface with convective boundary condition were analyzed by Akbar et al. [8]. Nadeem et al. [9] examined the MHD three-dimensional boundary layer flow of Casson nanofluid past a linearly stretching sheet with

Table 2 Values of C_{fx}, Nu_x, and Sh_x for different Sc, Pr and ξ ($\beta_e = 0.5$, $\beta_i = 0.4$, $\varepsilon = 0.1$, $\delta = 0.3$, $Gr = 1.0$, $Ec = Da = Fs = 0.1$, $N_m = N = 0.5$).

Sc	Pr	$\xi = 1.0$			$\xi = 2.0$			$\xi = 3.0$		
		C_{fx}	Nu_x	Sh_x	C_{fx}	Nu_x	Sh_x	C_{fx}	Nu_x	Sh_x
0.25	7.0	0.2614	0.5244	0.1617	0.0758	0.1115	0.1727	0.0346	0.1962	0.1989
0.75		0.2614	0.5235	0.1645	0.0757	0.1110	0.1852	0.0346	0.1937	0.2015
0.98		0.2612	0.5202	0.1751	0.0756	0.1106	0.1884	0.0344	0.1893	0.2061
1.25		0.2612	0.5185	0.1849	0.0755	0.1099	0.1899	0.0344	0.1825	0.2101
2.0		0.2607	0.5157	0.2202	0.0755	0.1096	0.1971	0.0345	0.1816	0.2124
0.6	0.71	0.2753	0.1544	0.1629	0.0755	0.1188	0.1929	0.0345	0.1936	0.2037
	1.0	0.2744	0.1777	0.1597	0.0754	0.1483	0.1928	0.0344	0.1978	0.2020
	2.0	0.2712	0.2610	0.1572	0.0753	0.1701	0.1927	0.0344	0.1987	0.2014
	3.0	0.2685	0.3294	0.1527	0.0753	0.1874	0.1926	0.0344	0.1994	0.1996
	5.0	0.2645	0.4359	0.1501	0.0753	0.1912	0.1925	0.0343	0.1996	0.1987

Table 3 Values of C_{fx}, Nu_x, and Sh_x for different δ, N_m, Fs and ξ ($\varepsilon = 0.1$, $\beta_e = 0.5$, $\beta_i = 0.4$, $Gr = 1.0$, $Ec = Da = 0.1 = Fs$, $N = 0.5$, $Sc = 0.6$, $Pr = 7.0$).

δ	N_m	Fs	$\xi = 1.0$			$\xi = 2.0$			$\xi = 3.0$		
			C_{fx}	Nu_x	Sh_x	C_{fx}	Nu_x	Sh_x	C_{fx}	Nu_x	Sh_x
0	0.5	0.1	0.2816	0.5111	0.1632	0.0802	0.0992	0.1886	0.0349	0.1573	0.1913
5			0.2823	0.5130	0.1635	0.0802	0.0985	0.1888	0.0349	0.1580	0.1908
10			0.2839	0.5142	0.1641	0.0808	0.1004	0.1894	0.0357	0.1619	0.1920
15			0.2858	0.5178	0.1628	0.0815	0.1007	0.1896	0.0364	0.1676	0.1930
20			0.2885	0.5197	0.1647	0.0824	0.1071	0.1933	0.0369	0.1872	0.2039
30			0.2970	0.5220	0.1652	0.0829	0.1096	0.1962	0.0380	0.2023	0.2183
0.3	0.01	0.1	0.2846	0.5265	0.1695	0.0831	0.1117	0.1934	0.0384	0.1908	0.2029
	0.25		0.2831	0.5231	0.1682	0.0830	0.1111	0.1930	0.0381	0.1880	0.2018
	0.75		0.2801	0.5162	0.1647	0.0826	0.1098	0.1921	0.0378	0.1818	0.1995
	1.0		0.2787	0.5128	0.1628	0.0825	0.1092	0.1917	0.0376	0.1791	0.1986
	1.2		0.2775	0.5102	0.1610	0.0823	0.1087	0.1914	0.0375	0.1767	0.1977
0.3	0.6	0.01	0.2813	0.5208	0.1700	0.0828	0.1072	0.1929	0.0379	0.1860	0.2018
		0.25	0.2806	0.5196	0.1691	0.0828	0.1077	0.1928	0.0379	0.1858	0.2012
		0.35	0.2800	0.5164	0.1676	0.0828	0.1086	0.1926	0.0379	0.1850	0.2022
		0.5	0.2791	0.5146	0.1665	0.0828	0.1083	0.1925	0.0378	0.1844	0.2021
		0.6	0.2785	0.5134	0.1635	0.0828	0.1082	0.1923	0.0378	0.1839	0.2010

convective boundary condition. Akbar et al. [10] investigated the MHD boundary layer flow of tangent hyperbolic fluid toward a stretching sheet using fourth and fifth order Rung e–Kutta–Fehlberg method. Hall currents and Ionslip effects become significant in strong magnetic fields and can considerably affect the current density in hydromagnetic heat transfer. Joule heating effects are also important and are caused by heating of the electrically-conducting fluid by the electrical current. As such considerable attention has been devoted to studying hydromagnetic convection flows with such effects. Hossain [11] reported on the effects of Hall currents on transient natural convection MHD boundary layer with suction at the wall using the Keller-Box numerical method. Raju and Rao [12] studied the cases of conducting and non-conducting walls for ionized hydromagnetic rotating heat transfer in a parallel plate channel with Hall currents. They showed that the temperature field is independent of partial pressure of electron gas for the case of non-conducting walls. Sawaya et al. [13] determined experimentally the Hall parameter for electrolytic solutions in a closed loop thermo symphonic magnetohydrodynamic flow system. A one dimensional theoretical model with the measured open circuit voltage was used to quantify Hall parameter. Bhargava and Takhar [14] studied computationally the influence of Hall currents on hydromagnetic heat transfer of a viscoelastic fluid in a channel. These studies did not consider however the presence of ion-slip currents. In weaker magnetic fields, the diffusion velocity of electrons and ions is different and usually ionslip effects are neglected. However in MHD generators and industrial materials processing where the electromagnetic body forces are large, the diffusion velocity of the ions cannot be neglected. When both electron and ion velocities are incorporated in the analysis, the ionslip phenomenon is present and Ohm's law has to be modified accordingly. An excellent discussion of ionslip effects has been presented by Cramer and Pai [15]. Soundalgekar et al. [16] were among the first researchers to consider ionslip effects in hydromagnetic Couette heat transfer in addition to Hall currents effects. They showed that for small magnetic field parameters or high ionslip and Hall current parameters, the flow can become unstable. Ram and Takhar [17] reported on the rotating natural convection MHD flow with Hall/ionslip current effects. Ram et al. [18] extended this study to consider

Table 4 Values of C_{fx}, Nu_x, and Sh_x for different Da, N and ξ ($\beta_e = 0.5$, $\beta_i = 0.4$, $\varepsilon = 0.1$, $\delta = 0.3$, $Gr = 1.0$, $Ec = Fs = 0.1$, $N_m = 0.5$, $Sc = 0.6$, $Pr = 7.0$).

Da	N	$\xi = 1.0$			$\xi = 2.0$			$\xi = 3.0$		
		C_{fx}	Nu_x	Sh_x	C_{fx}	Nu_x	Sh_x	C_{fx}	Nu_x	Sh_x
0.05	0.5	0.1939	0.3545	0.1640	0.0536	0.1098	0.1903	0.0245	0.1684	0.1892
0.06		0.2105	0.3927	0.1647	0.0587	0.1123	0.1921	0.0268	0.1744	0.1995
0.08		0.2383	0.4658	0.1647	0.0677	0.1146	0.1929	0.0309	0.1818	0.1971
0.1		0.2614	0.5196	0.1653	0.0755	0.1209	0.1957	0.0344	0.1880	0.2003
0.12		0.2812	0.5685	0.1673	0.0825	0.1268	0.1958	0.0376	0.1972	0.2012
0.15		0.3063	0.6283	0.1688	0.0921	0.1358	0.1895	0.0421	0.2012	0.2072
0.1	0.0	0.1745	0.3974	0.1556	0.0505	0.1087	0.1895	0.0231	0.1722	0.1978
	0.1	0.1918	0.4234	0.1565	0.0555	0.1088	0.1915	0.0253	0.1799	0.2006
	0.3	0.2265	0.4734	0.1735	0.0655	0.1115	0.1935	0.0299	0.1882	0.2015
	0.8	0.3142	0.5816	0.1819	0.0905	0.1173	0.1942	0.0413	0.1920	0.2018
	1.0	0.3494	0.6185	0.1852	0.1004	0.1215	0.1951	0.0457	0.1947	0.2022

Table 5 KBM and NTM solutions compared for C_{fx}, Nu_x, and Sh_x for different β_e and ξ ($\beta_i = 0.4$, $\varepsilon = 0.1$, $\delta = 0.3$, $N_m = 0.5$, $Sc = 0.6$, $Gr = 1.0$, $Fs = Ec = Da = 0.1$, $N = 0.5$, $Pr = 7.0$).

β_e	$\xi = 1.0$			$\xi = 1.0$		
	C_{fx} KBM	Nu_x KBM	Sh_x KBM	C_{fx} NTM	Nu_x NTM	Sh_x NTM
0.1	0.2806	0.5171	0.1658	0.2805	0.5173	0.1660
0.5	0.2818	0.5200	0.1645	0.2817	0.5202	0.1647
1.0	0.2826	0.5220	0.1635	0.2824	0.5223	0.1637
2.0	0.2836	0.5251	0.1623	0.2834	0.5254	0.1625
3.0	0.2840	0.5258	0.1618	0.2838	0.5260	0.1620
5.0	0.2843	0.5423	0.1614	0.2840	0.5425	0.1616

Table 6 KBM and NTM solutions compared for C_{fx}, Nu_x, and Sh_x for different β_i and ξ ($\beta_e = 0.5$, $\varepsilon = 0.1$, $\delta = 0.3$, $N_m = 0.5$, $Sc = 0.6$, $Gr = 1.0$, $Fs = Ec = Da = 0.1$, $N = 0.5$, $Pr = 7.0$).

β_i	$\xi = 1.0$			$\xi = 1.0$		
	C_{fx} KBM	Nu_x KBM	Sh_x KBM	C_{fx} NTM	Nu_x NTM	Sh_x NTM
0.0	0.2812	0.5185	0.1617	0.2810	0.5186	0.1618
1.0	0.2821	0.5208	0.1620	0.2820	0.5209	0.1621
3.0	0.2830	0.5230	0.1624	0.2829	0.5231	0.1625
5.0	0.2834	0.5241	0.1629	0.2833	0.5242	0.1630
8.0	0.2838	0.5248	0.1641	0.2837	0.5249	0.1642
12.0	0.2840	0.5254	0.1652	0.2839	0.5255	0.1653

the effects of oscillating wall temperature using a numerical method. Further studies of combined Hall and ionslip currents in magnetohydrodynamic heat transfer flows were provided by Takhar and Jha [19] and more recently by Anwar Beg et al. [20]. Several studies of Joule electrical heating in MHD heat transfer flows have also appeared. Mansour and Gorla [21] studied the effects of Joule heating effects on transient free hydromagnetic convection in a micropolar fluid. Bég [22] studied the effects of Joule heating in MHD channel flow using a Navier–Stokes computational solver. Aissa and Mohammadein [23] more recently analyzed the effects of Joule heating and variable electric conductivity on micropolar stretching flow and heat transfer using a shooting numerical scheme. The combined effects of Hall current, magnetic induction and oblique magnetic field on MHD flow in a spinning channel with heat transfer were studied by Ghosh et al. [24]. Other studies incorporating Joule heating have been communicated by Duwairi [25] and Bég et al. [26] who employed an electrothermal network simulation code.

In many industrial and geophysical flows viscous dissipation effects may also arise owing to internal friction in viscous fluids which can affect temperature fields. Many studies have been reported concerning viscous heating effects in both natural and forced convection heat transfer flows. These include the articles by Gebhart and Mollendorf [27] and Soundalgekar and Pop [28] which dwell on boundary layer heat transfer. In hydromagnetic heat transfer several studies have been reported concerning viscous heating effects. Javeri [29] studied hydromagnetic heat transfer in a channel with the collective effects of Hall current, ion slip, viscous dissipation and Joule heating. Takhar and Soundalgekar [30] presented numerical solutions for the effects of Eckert number (viscous heating parameter) on hydromagnetic natural convection boundary layer flow. Other non-magnetic studies of viscous heating effects include those by Turcotte et al. [31], Basu and Roy [32], Barletta [33] and Barletta and Rossi di Schio [34]. These studies have all been restricted to purely fluid regimes. In numerous systems the medium may be a porous material. The porosity of materials is an intrinsic aspect of many chemical engineering and materials processing systems. Ceramics, batch reactors, purification systems and filtration systems all utilize porosity. Traditionally, the Darcian model has been employed to analyze most convection flows in porous media. Such a model however is generally only accurate at very low Reynolds numbers and cannot simulate the inertial effects experienced at higher Reynolds numbers. Engineers have therefore extended the Darcian model to incorporate second order drag force effects generally with the Forchheimer-extended Darcian model, which is easily implemented in boundary layer heat transfer analysis. Excellent studies of Darcy–Forchheimer convection in porous media have been presented by for example, Chen and Ho [35] and also Manole and Lage [36].

An interesting non-Newtonian model developed for chemical engineering systems is the *Eyring–Powell* fluid model. This

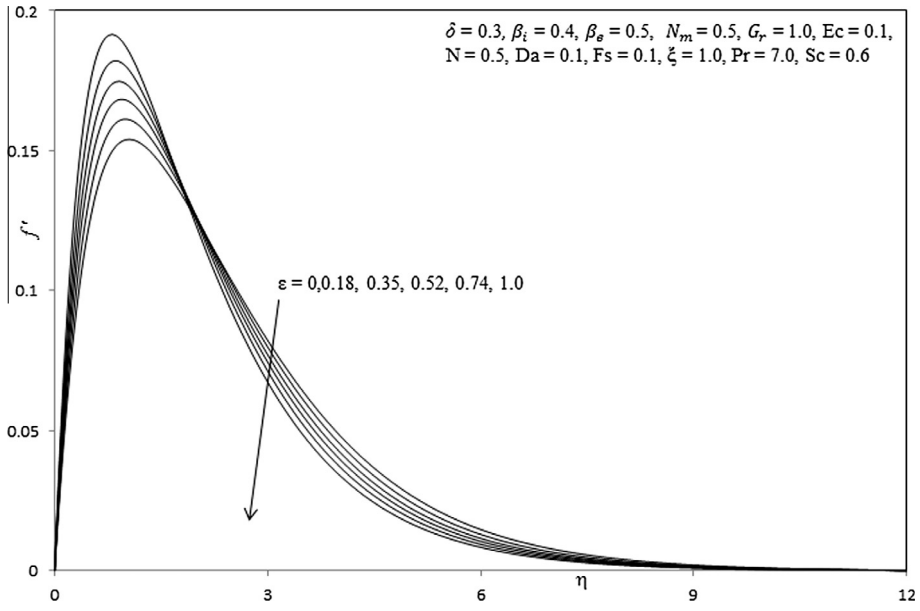

Figure 2a Influence of ε on primary velocity profiles.

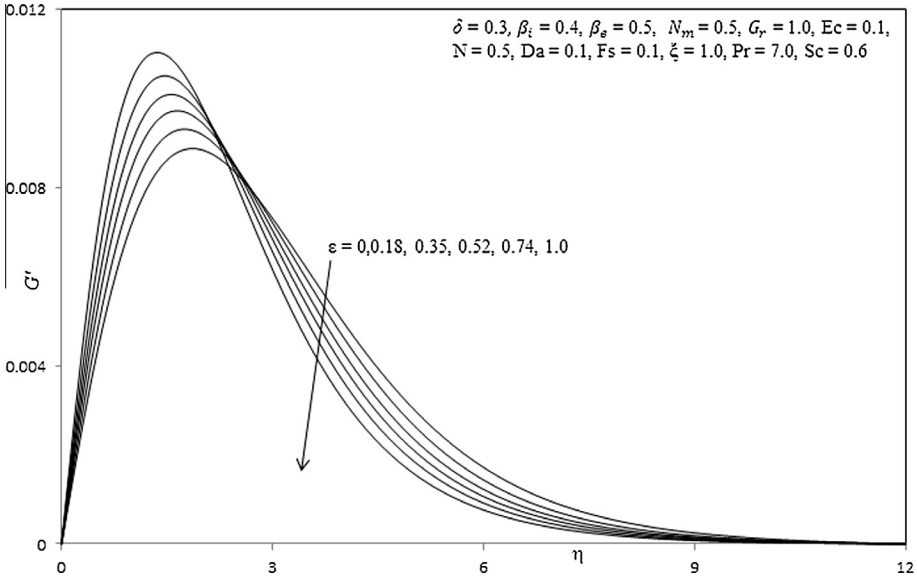

Figure 2b Influence of ε on secondary velocity profiles.

rheological model has certain advantages over the other non-Newtonian formulations, including simplicity, ease of computation and physical robustness. Furthermore, it is deduced from kinetic theory of liquids rather than the empirical relation. Additionally, it correctly reduces to Newtonian behavior for low and high shear rates [37]. Several communications utilizing the Eyring–Powell fluid model have been presented in the scientific literature. Zueco and Bég [38] numerically studied the pulsatile flow of Eyring–Powell model using the network electro-thermal solver code, PSPICE. Islam et al. [39] derived homotopy perturbation solutions for slider bearings lubricated with Eyring–Powell fluids. Patel and Timol [40] numerically examined the flow of Eyring–Powell fluids from a two-dimensional wedge. Further investigations implementing the Eyring–Powell model in transport phenomena include Ramachandra Prasad et al. [41] for vertical porous plate flows, Akbar et al. [42] for peristaltic thermal convection flows of reactive biofluids, Hayat et al. [43] for Sakiadis flows and Abdul Gaffar et al. [3] for wedge flows. The Eyring–Powell model was also deployed by Yürüsoy [44] to investigate bearing tribological flows, by Ai and Vafai [45] to simulate Stokesian impulsively-started plate flows and also by Adesanya and Gbadeyan [46] for channel flows. Recent work on Eyring–Powell fluid includes Abdul Gaffar et al. [47].

The above studies however did not consider the mass transfer and the *collective effects* of Joule heating, Hall/ionslip currents in porous media transport phenomena. The vast majority of simulations employ a *Darcian* model [48], valid for viscous-

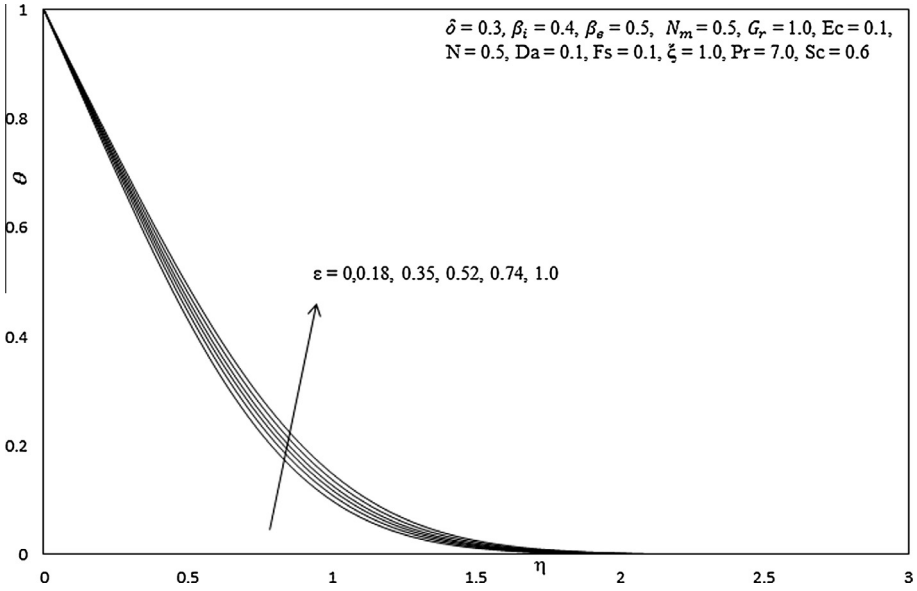

Figure 2c Influence of ε on temperature profiles.

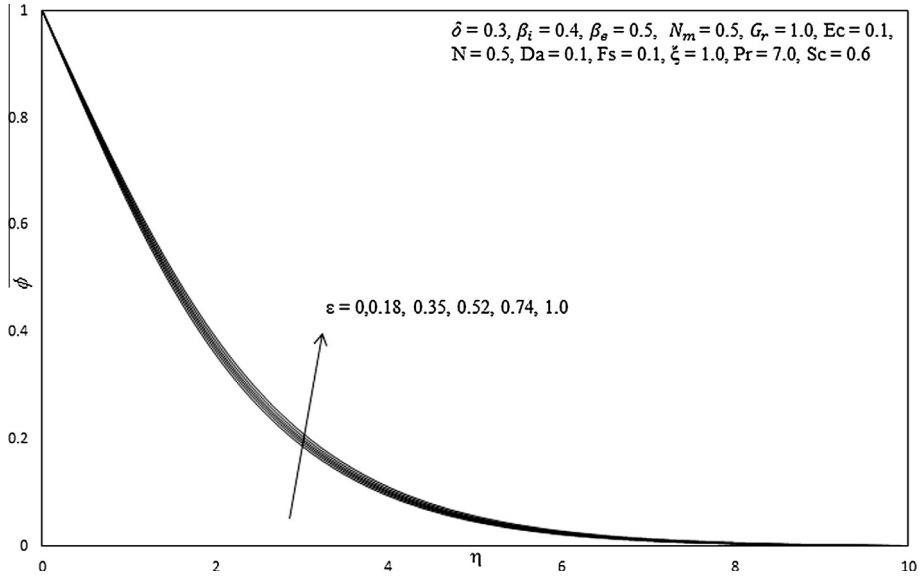

Figure 2d Influence of ε on concentration profiles.

dominated flows. In this paper we shall therefore, consider the *composite effects of Joule heating, Hall and ionslip currents, and also viscous frictional heating on two-dimensional natural MHD convection of Eyring–Powell Fluid in a Darcy-Forchheimer porous medium from a vertical plate*. Such a study has thus far not appeared in the literature and constitutes a useful extension to the current body of work on non-linear magneto-convective transport phenomena in porous media.

2. Non-newtonian constitutive Eyring–Powell fluid model

In the present study a subclass of non-Newtonian fluids known as *Eyring–Powell fluid* is employed owing to its simplicity. The Cauchy stress tensor, in *as Eyring–Powell* fluid [37] takes the following form:

$$\tau_{ij} = \mu \frac{\partial u_i}{\partial x_j} + \frac{1}{\beta} \sinh^{-1}\left(\frac{1}{C}\frac{\partial u_i}{\partial x_j}\right) \tag{1}$$

where μ is dynamic viscosity, and β and C are the rheological fluid parameters of the Eyring–Powell fluid model. Consider the second-order approximation of the $\sinh^{-1}$ function as follows:

$$\sinh^{-1}\left(\frac{1}{C}\frac{\partial u_i}{\partial x_j}\right) \cong \frac{1}{C}\frac{\partial u_i}{\partial x_j} - \frac{1}{6}\left(\frac{1}{C}\frac{\partial u_i}{\partial x_j}\right)^3, \quad \left|\frac{1}{C}\frac{\partial u_i}{\partial x_j}\right| \ll 1 \tag{2}$$

The introduction of the appropriate terms into the flow model is considered next. The resulting boundary value problem is found to be well-posed and permits an excellent mechanism for the assessment of rheological characteristics on the flow behavior.

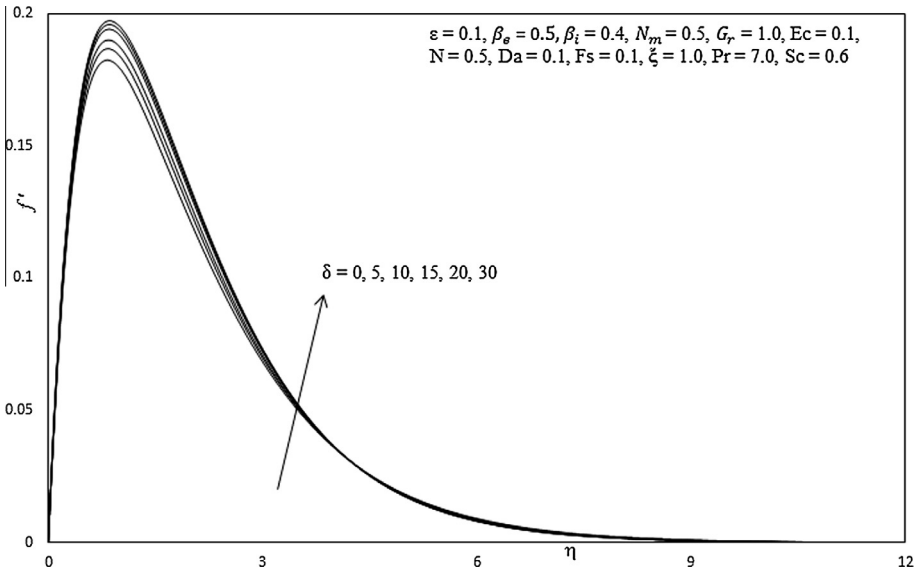

Figure 3a Influence of δ on primary velocity profiles.

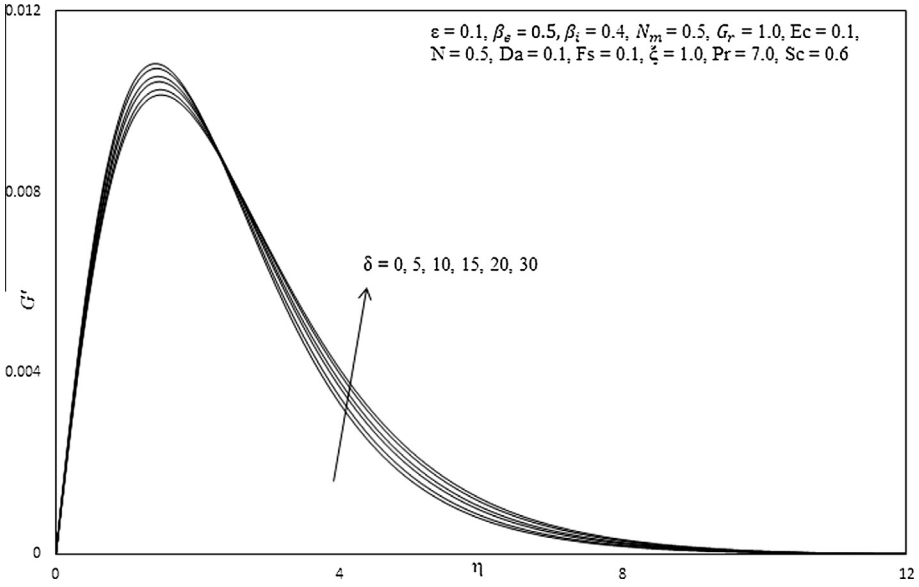

Figure 3b Influence of δ on secondary velocity profiles.

3. Mathematical model

We consider the steady-state hydromagnetic natural convection flow of a viscous, incompressible, partially-ionized, electrically-conducting flow of *Eyring–Powell fluid* adjacent to a non-isothermal, vertical surface in an (x, y, z) coordinate system embedded in a non-Darcy saturated porous medium. The plate surface is in the x–z plane. The z-axis coincides with the leading edge of the plate. A strong magnetic field acts parallel to the y-axis. The physical model is illustrated in Fig. 1. The magnetic Reynolds number is small for the partially-ionized fluid so that magnetic induction effects can be ignored. However, relative motion of the particles in the fluid can occur and the electron-atom collision frequency is assumed to be high enough for Hall and ionslip currents to be significant. As such, an electric current density, $\boldsymbol{J}$, is required to represent the relative motion of charged particles. Considering only the electromagnetic forces on these particles, we can utilize the generalized Ohm law. With a magnetic field, $\boldsymbol{B}$, applied normal to the electrical field $\boldsymbol{E}$, an electromagnetic force is generated normal to both $\boldsymbol{E}$ and $\boldsymbol{B}$ in the z direction. Such a force causes charged particles to migrate perpendicularly to both $\boldsymbol{E}$ and $\boldsymbol{B}$ [15]. Consequently, a component of electrical current density exists perpendicular to both $\boldsymbol{E}$ and $\boldsymbol{B}$, and this constitutes the Hall current. For a strong magnetic field $\boldsymbol{B}$ the diffusion velocity of the ions will be significant, constituting the ionslip effect. From the equation of conservation of electrical charge:

$$\nabla \cdot \boldsymbol{J} = 0 \tag{4}$$

where $\boldsymbol{J} = (J_x, J_y, J_z)$. Since the plate is not composed of electrically-conducting material, electrical charge at the surface of the plate is constant and zero i.e. $J_y \to 0$. Consequently we

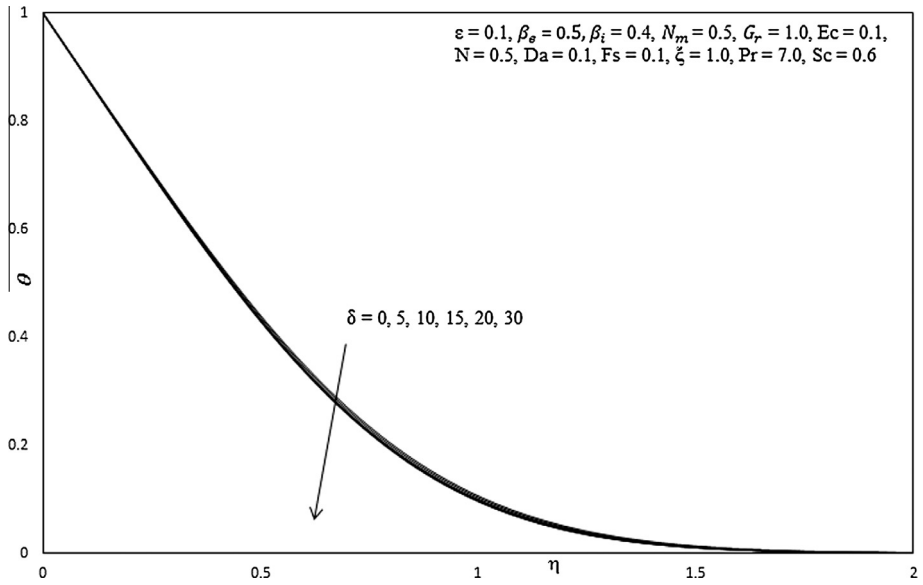

Figure 3c Influence of δ on temperature profiles.

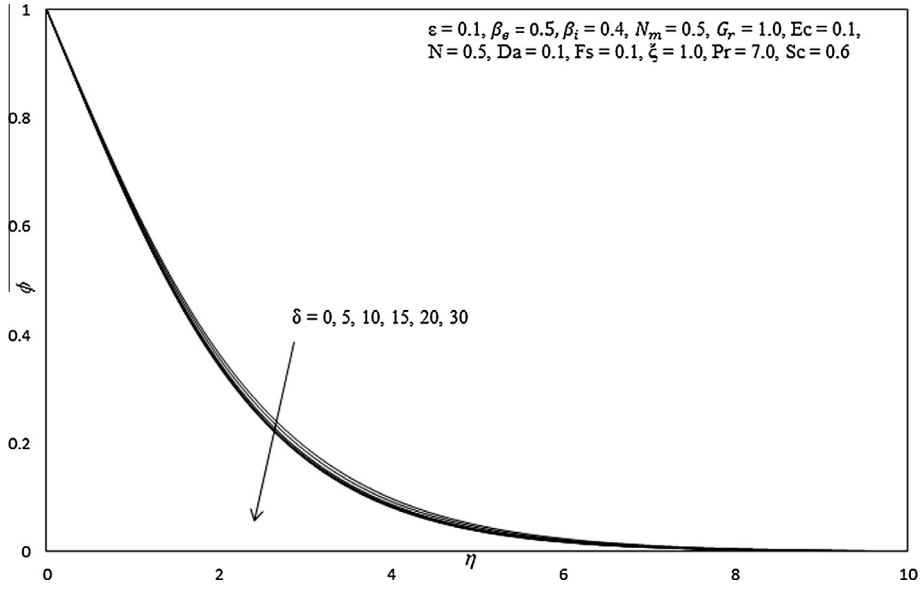

Figure 3d Influence of δ on concentration profiles.

can assume that $J_y = 0$ throughout the fluid-saturated porous medium. The magnetic field acts only in the y-direction with a component, B_o. Both the vertical surface and the *Eyring–Powell fluid* are maintained initially at the same temperature and concentration. Instantaneously, they are raised to a temperature T_w ($> T_\infty$) and concentration C_w ($> C_\infty$), the ambient temperature and concentration of the fluid which remain unchanged. We implement a Darcy–Forchheimer model which is a second order relationship defining the pressure gradient as follows:

$$\nabla p = -aU + bU^2 \tag{5}$$

where U denotes velocity, ∇p is pressure gradient, a and b are constants defined by $a = \mu/K$ and b is a function of the geometry of porous medium i.e. $b = \rho/K_1$ is the Forchheimer form-drag parameter for quadratic effects, μ is the dynamic viscosity of the partially-ionized fluid, K is permeability [hydraulic conductivity] of the porous medium and K_1 is the inertial permeability. We assume that the density of the partially-ionized fluid can be taken as constant i.e. the flow is incompressible. In addition, we implement the Boussinesq approximation which implies that all thermodynamic quantities of the fluid-saturated medium are constant, except for the buoyancy term, which is retained in the x-direction momentum conservation equations. We have assumed that the porous medium is homogenous and isotropic so that only a single permeability is needed to simulate hydraulic conductivity. Under these physical conditions, with viscous and Joule heating effects

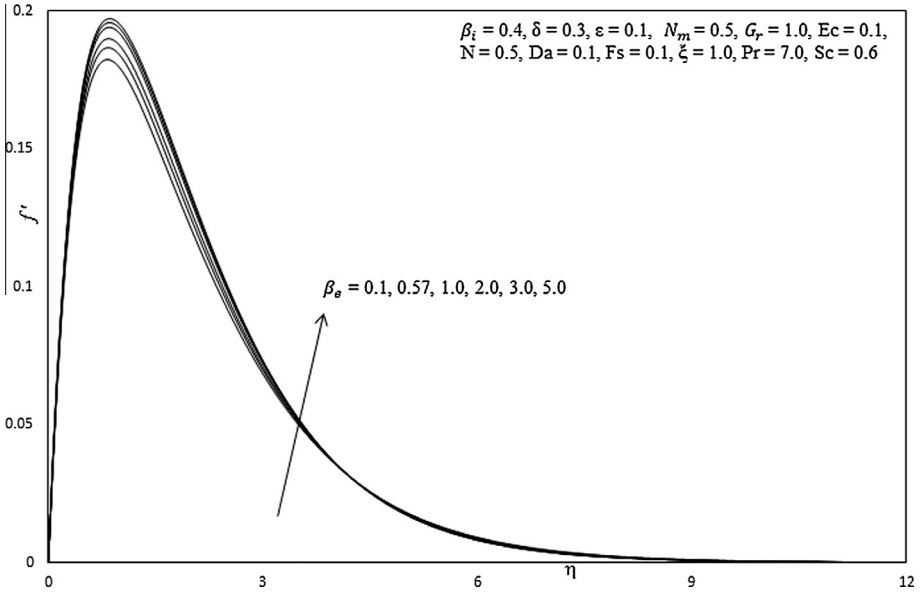

Figure 4a Influence of β_e on primary velocity profiles.

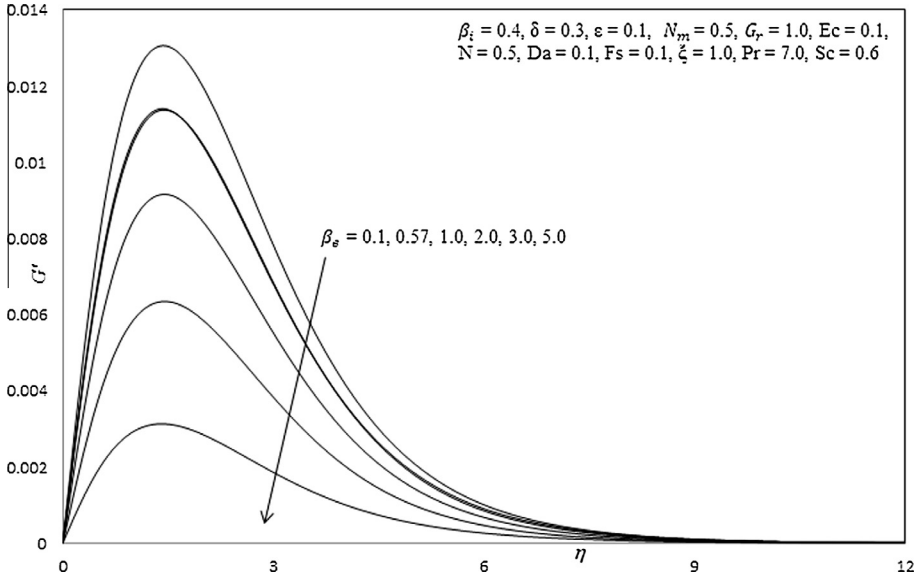

Figure 4b Influence of β_e on secondary velocity profiles.

incorporated, the flow regime in an $[x, y, z]$ coordinate system can be represented by the following boundary-layer equations:

$$\frac{\partial u}{\partial x}+\frac{\partial v}{\partial y}=0 \tag{6}$$

$$u\frac{\partial u}{\partial x}+v\frac{\partial u}{\partial y}=\left[v+\frac{1}{\rho\beta C_1}\right]\frac{\partial^2 u}{\partial y^2}-\frac{1}{2\rho\beta C_1^3}\left(\frac{\partial u}{\partial y}\right)^2\frac{\partial^2 u}{\partial y^2}+g\beta_1[T-T_\infty]+g\beta_1^*[C-C_\infty]-v\frac{u}{K}-b\frac{u^2}{K}-\frac{\sigma B_o^2}{\rho(\alpha_e^2+\beta_e^2)}(\alpha_e u+\beta_e w) \tag{7}$$

$$u\frac{\partial w}{\partial x}+v\frac{\partial w}{\partial y}=\left[v+\frac{1}{\rho\beta C_1}\right]\frac{\partial^2 w}{\partial y^2}-\frac{1}{2\rho\beta C_1^3}\left(\frac{\partial w}{\partial y}\right)^2\frac{\partial^2 w}{\partial y^2}-v\frac{w}{K}-b\frac{w^2}{K}+\frac{\sigma B_o^2}{\rho(\alpha_e^2+\beta_e^2)}(\beta_e u-\alpha_e w) \tag{8}$$

$$u\frac{\partial T}{\partial x}+v\frac{\partial T}{\partial y}=\frac{k}{\rho c_p}\frac{\partial^2 T}{\partial y^2}+\frac{v}{c_p}\left[\left(\frac{\partial u}{\partial y}\right)^2+\left(\frac{\partial w}{\partial y}\right)^2\right]+\frac{\sigma B_o^2}{\rho c_p(\alpha_e^2+\beta_e^2)}(u^2+w^2) \tag{9}$$

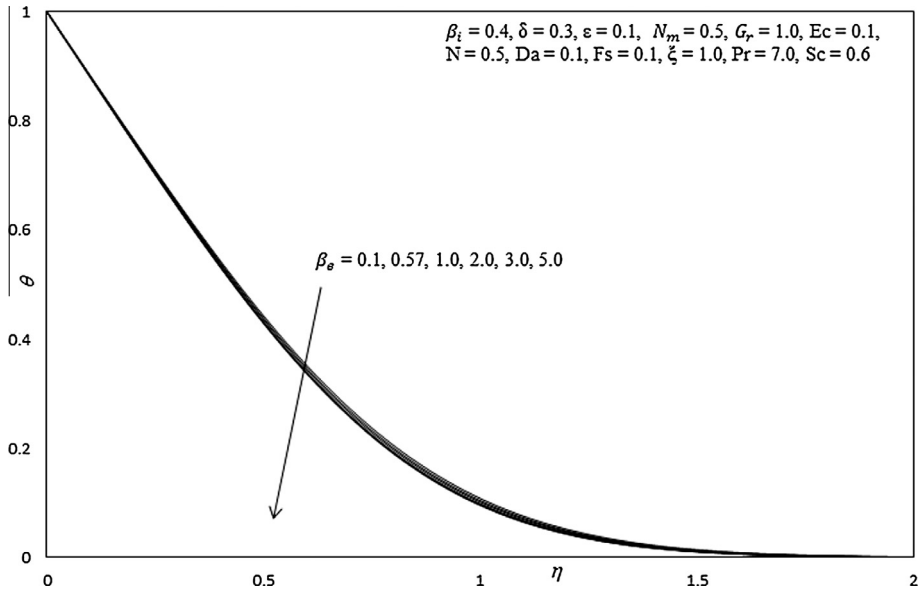

Figure 4c Influence of β_e on temperature profiles.

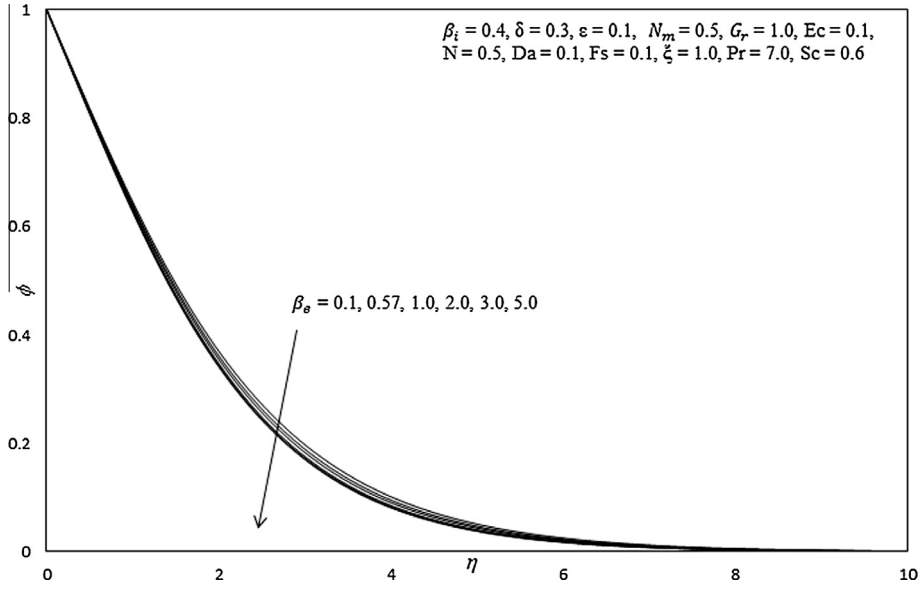

Figure 4d Influence of β_e on concentration profiles.

$$u\frac{\partial C}{\partial x}+v\frac{\partial C}{\partial y}=D_m\frac{\partial^2 C}{\partial y^2} \tag{10}$$

where u, v, w are velocity components in the x, y, z directions, T is the fluid temperature, C is the fluid concentration, v is kinematic viscosity of the partially-ionized fluid, g is acceleration due to gravity, K is the thermal diffusivity, b is the inertial drag coefficient, C_1 is the fluid parameter, β is the fluid parameter, β_1 is the coefficient of thermal expansion, β_1^* is the coefficient of expansion with concentration, ρ is density of the electrically-conducting fluid, k is thermal conductivity of the fluid-saturated porous medium, D_m, is the mass (species) diffusivity, c_p is specific heat capacity of the fluid under isobaric conditions, σ is the fluid electrical conductivity ($=e^2t_en_e/m_e$), e denotes the electron charge, t_e is the electron collision time, n_e is the electron number density, m_e is the electron mass, $\alpha_e = 1 + \beta_i\beta_e$, $\beta_i = \frac{en_eB_o}{\left[\left(1+\frac{n_e}{n_a}\right)K_{ai}\right]}$ is the ion-slip parameter, $\beta_e = \omega_e t_e$ is the Hall current parameter, ω_e is the electron frequency ($=eB_o/m_e$), n_a is the neutral particle number density and K_{ai} is the friction coefficient between the ions and neutral particles in the flow. The Eyring–Powell fluid model introduces a mixed derivative (second order, first degree) into the momentum boundary layer Eq. (7). In Eq. (7) the fifth and sixth terms on the right hand side are the *x-direction Darcian drag force* and the *x-direction Forchheimer quadratic drag*. Similar terms are incorporated for the z-direction components of these forces in Eq. (8). We note that the viscous heating term in (9) comprises the square of two velocity gradients $\left[\left(\frac{\partial u}{\partial y}\right)^2+\left(\frac{\partial v}{\partial y}\right)^2\right]$

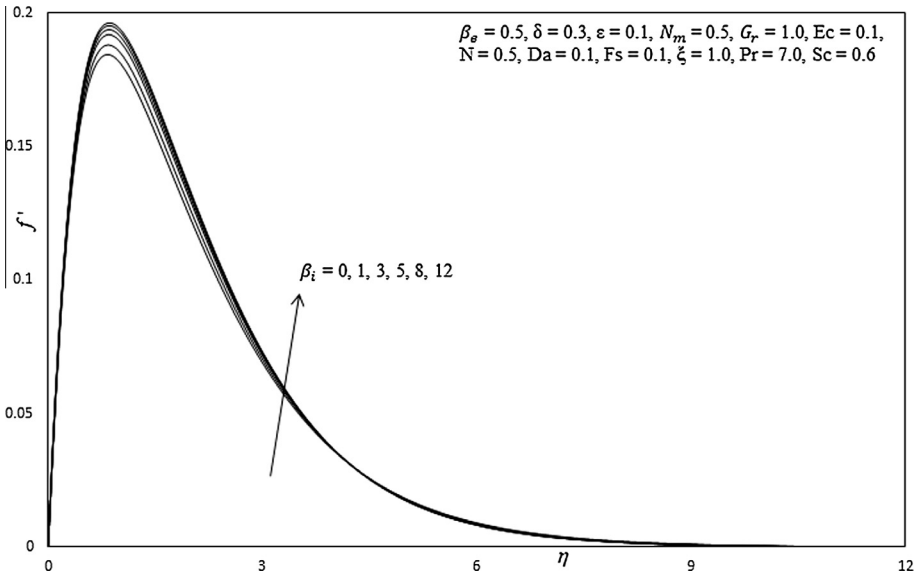

Figure 5a Influence of β_i on primary velocity profiles.

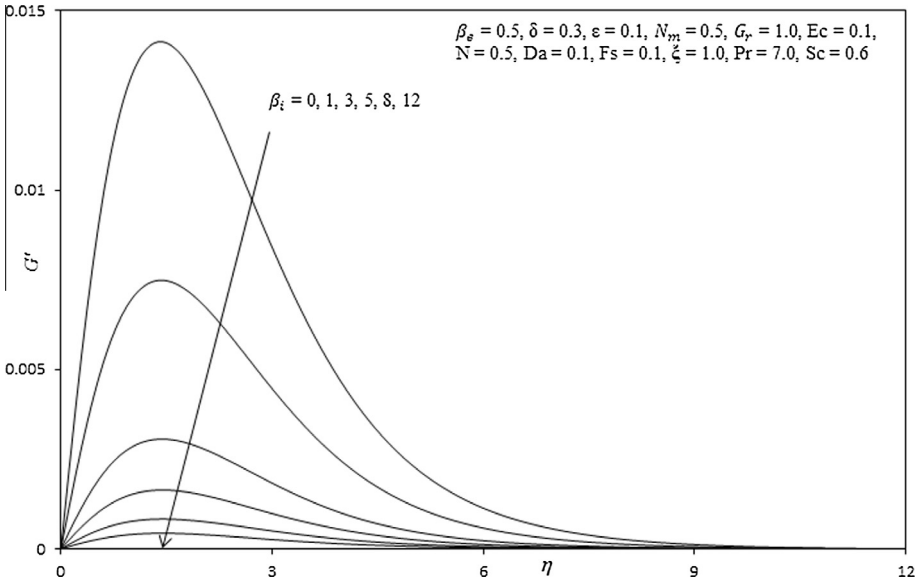

Figure 5b Influence of β_i on secondary velocity profiles.

which is a realistic approximation, supported by the seminal study of Gebhart and Mollendorf [27]. The corresponding initial conditions and boundary conditions for the flow regime are prescribed as follows, which include the conventional no-slip boundary condition at the plate surface:

$$\text{At } y = 0: \quad u = v = 0,\ w = 0,\ T = T_w,\ C = C_w \tag{11a}$$

$$\text{As } y \to \infty: \quad u \to 0,\ w \to 0,\ T \to T_\infty,\ C \to C_\infty \tag{11b}$$

Here T_∞ and C_∞ are free stream temperature and concentration respectively.

To transform the boundary value problem to a dimensionless one, i.e. coupled non-linear partial differential Eqs. (6)–(10) under conditions (11a,b), we introduce a stream function Ψ defined by the Cauchy–Riemann equations, $u = \frac{\partial \psi}{\partial y}$ and $v = -\frac{\partial \psi}{\partial x}$, and therefore, the mass conservation Eq. (6) is automatically satisfied. Furthermore, the following dimensionless variables are introduced into Eqs. (6)–(10) and (11a,b):

$$\eta = \frac{C_1 y}{x^{1/4}}, \quad \xi = \frac{x^{1/2}}{L^{1/2}}, \quad \Psi = 4\nu C_1 x^{3/4} f(\xi, \eta),$$
$$w = 4\nu C_1^2 x^{1/2} G(\xi, \eta), \quad \varepsilon = \frac{1}{\mu\beta C_1}, \quad \delta = 8\nu^2 C_1^3 L^{1/2}$$
$$\theta = \frac{T - T_\infty}{T_w - T_\infty}, \quad \phi = \frac{C - C_\infty}{C_w - C_\infty}, \quad Pr = \frac{\mu c_p}{k},$$
$$Gr_x = \frac{g\beta x^3 [T_w - T_\infty]}{\nu^2}, \quad Ec = \frac{4L\nu^2 C_1^4}{c_p [T_w - T_\infty]}$$
$$Nm = \frac{\sigma B_o^2 L^{1/2}}{2\rho\nu C_1^2}, \quad Da = \frac{K}{L^2}, \quad Fs = \frac{b}{L}, \quad Sc = \frac{\nu}{D_m},$$
$$C_1 = \left\{ \frac{g\beta [T_w - T_\infty]}{4\nu^2} \right\}^{1/4} \tag{12}$$

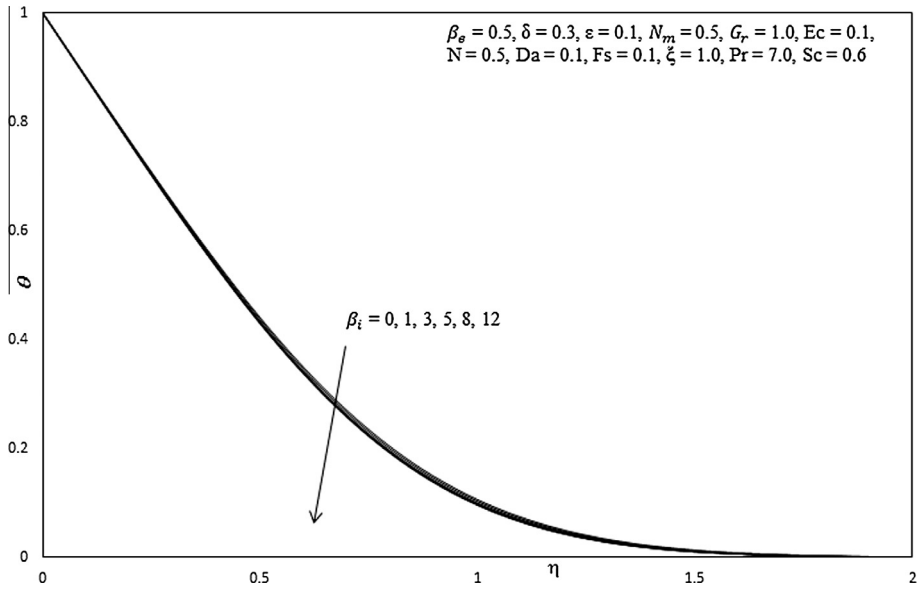

Figure 5c Influence of β_i on temperature profiles.

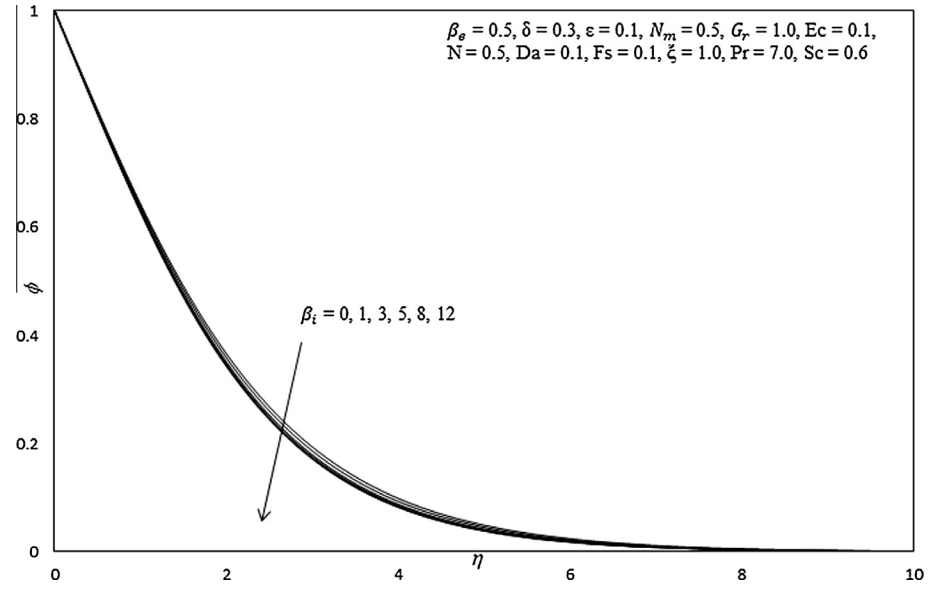

Figure 5d Influence of β_i on concentration profiles.

where L denotes a characteristic length, F is dimensionless stream function, G is dimensionless lateral velocity, θ is dimensionless temperature, ϕ is dimensionless concentration, ξ is dimensionless tangential coordinate, η is the dimensionless normal coordinate, Ψ is dimensionless stream function, N_m is the magnetic body force parameter, Pr is Prandtl number, Gr_x is local Grashof number, Ec is Eckert (viscous heating) number, Da is Darcy number, ε is the Eyring–Powell fluid parameter, δ is the local non-Newtonian fluid parameter, the local non-Newtonian parameter based on length scale, and Fs is Forchheimer (inertial) parameter. The resulting momentum, energy and concentration boundary layer equations take the following form:

$$(1+\varepsilon)f''' + 3ff'' - 2f'^2 - \varepsilon\delta\,\xi(f'')^2 f''' + (\theta + N\phi) - \frac{2}{Da\,Gr_x^{1/2}}\xi^4 f' - \frac{4Fs}{Da}\xi^2 f'^2 - \frac{2Nm}{[\alpha_e^2+\beta_e^2]}\xi[\alpha_e f' + \beta_e G] = 2\xi\left[f'\frac{\partial f'}{\partial \xi} - f''\frac{\partial f}{\partial \xi}\right] \tag{13}$$

$$(1+\varepsilon)G'' + 3fG' - 2Gf' - \varepsilon\delta\,\xi(G')^2 G'' - \frac{2}{Da\,Gr_x^{1/2}}\xi^4 G - \frac{4Fs}{Da}\xi^2 G^2 - \frac{2Nm}{[\alpha_e^2+\beta_e^2]}\xi[\alpha_e f' + \beta_e G] = 2\xi\left[f'\frac{\partial f'}{\partial \xi} - f''\frac{\partial f}{\partial \xi}\right] \tag{14}$$

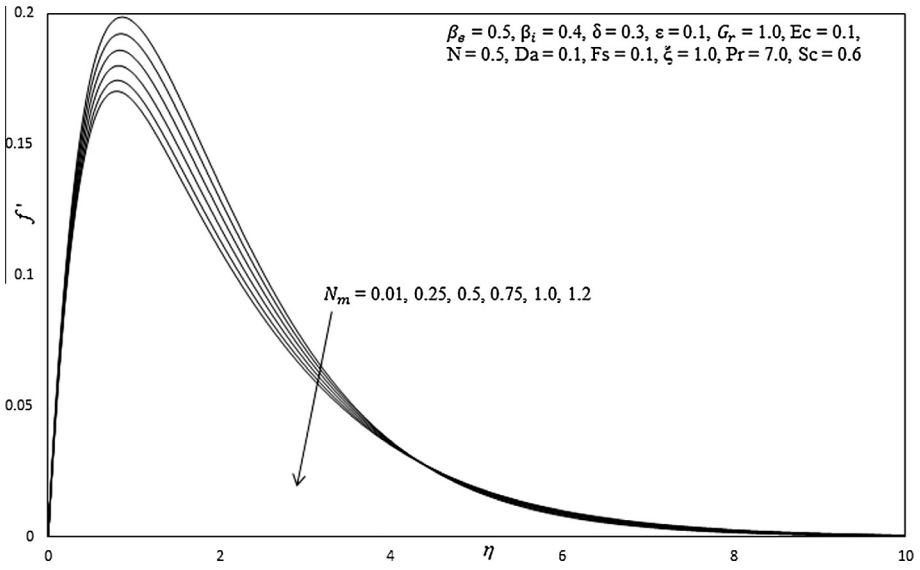

Figure 6a Influence of N_m on primary velocity profiles.

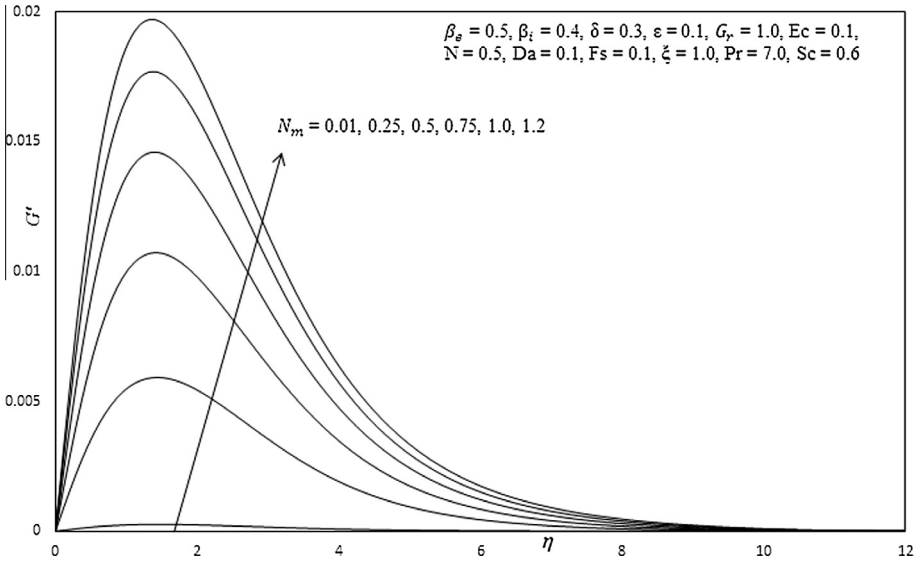

Figure 6b Influence of N_m on secondary velocity profiles.

$$\frac{1}{Pr}\theta'' + 3f\theta' + 4\xi^2 Ec[f''^2 + G'^2] + \frac{2N_m\, Ec}{[\alpha_e^2 + \beta_e^2]}\xi^3[f'^2 + G^2] = 2\xi\left[f\frac{\partial\theta}{\partial\xi} - \theta'\frac{\partial f}{\partial\xi}\right] \tag{15}$$

$$\frac{1}{Sc}\phi'' + 3f\phi' = 2\xi\left[f'\frac{\partial\phi}{\partial\xi} - \phi'\frac{\partial f}{\partial\xi}\right] \tag{16}$$

The corresponding transformed non-dimensional boundary conditions take the following form:

$$\text{At}\quad \eta = 0,\quad f = 0,\quad u = 0,\quad G = 0,\quad \theta = 0,\quad \phi = 0 \tag{17a}$$

$$\text{As}\quad \eta \to \infty,\quad f' \to 0,\quad G \to 0,\quad \theta \to 0,\quad \phi \to 0 \tag{17b}$$

Here primes denote the differentiation with respect to η.

4. Engineering parameters

For practical design purposes in MHD energy systems a number of engineering parameters provide important descriptions of the wall transport processes. The local heat flux, $q_w(x)$, local heat transfer coefficient, $h(x)$ at the wall and the heat transfer rate, Nu_x are defined as follows:

$$q_w(x) = -k\left.\frac{\partial T}{\partial y}\right|_{y=0} = -k[T_w - T_\infty]\frac{C_1}{x^{1/4}}\frac{\partial\theta(\xi,0)}{\partial\eta} \tag{18}$$

$$h(x) = \frac{q_w(x)}{[T_w - T_\infty]} = -k\frac{C_1}{x^{1/4}}\frac{\partial\theta(\xi,0)}{\partial\eta} \tag{19}$$

$$Nu_x = \frac{xh(x)}{k} = -\frac{1}{\sqrt{2}}Gr_x^{1/4}\frac{\partial\theta(\xi,0)}{\partial\eta} \tag{20}$$

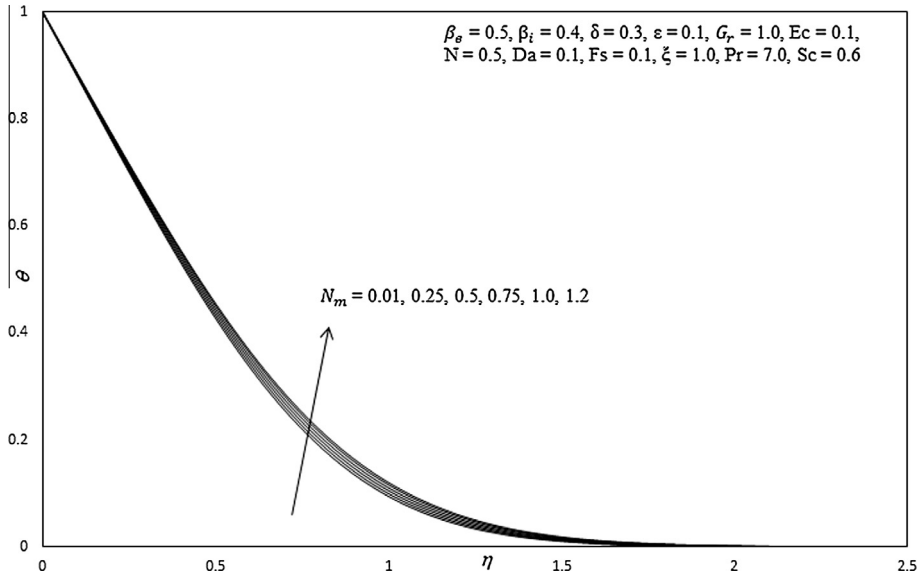

Figure 6c Influence of N_m on temperature profiles.

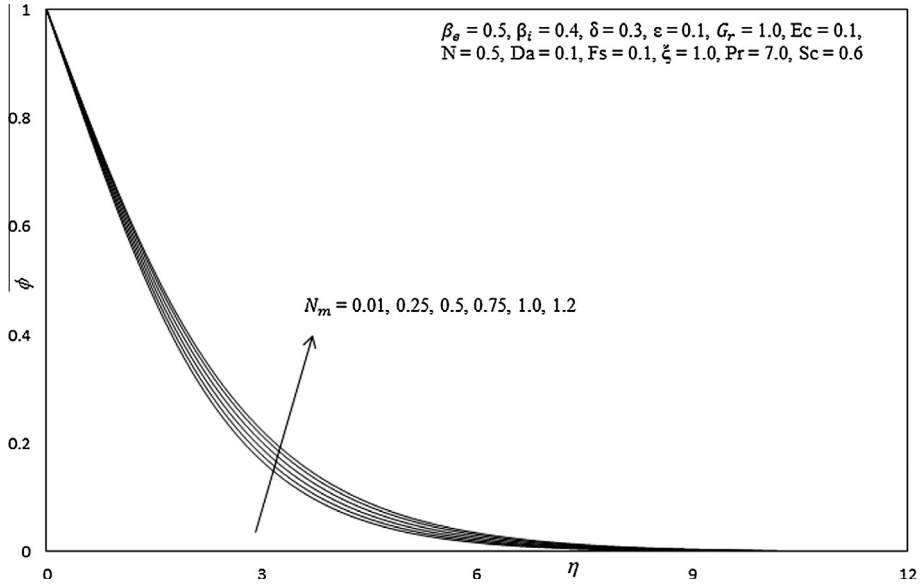

Figure 6d Influence of N_m on concentration profiles.

The local shear stress components in the x and z-directions respectively, namely, τ_{wx} and τ_{wz}, may be defined using the following relations:

$$\tau_{wx} = \sqrt{2}\,\mu v \frac{Gr_x^{3/4}}{x^2}\left[(1+\varepsilon)\frac{\partial^2 f(\xi,0)}{\partial \eta^2} - \frac{\varepsilon\delta}{3}\xi\left(\frac{\partial^2 f(\xi,0)}{\partial \eta^2}\right)^3\right] \quad (21a)$$

$$\tau_{wz} = \sqrt{2}\,\mu v \frac{Gr_x^{3/4}}{x^2}\left[(1+\varepsilon)\frac{\partial G(\xi,0)}{\partial \eta} - \frac{\varepsilon\delta}{3}\xi\left(\frac{\partial G(\xi,0)}{\partial \eta}\right)^3\right] \quad (21b)$$

The dimensionless skin friction coefficients in x and z-directions respectively, namely, C_{fx} and C_{gz} are defined as,

$$C_{fx} = (1+\varepsilon)\frac{\partial^2 f(\xi,0)}{\partial \eta^2} - \frac{\varepsilon\delta}{3}\xi\left(\frac{\partial^2 f(\xi,0)}{\partial \eta^2}\right)^3 \quad (22a)$$

$$C_{gz} = (1+\varepsilon)\frac{\partial G(\xi,0)}{\partial \eta} - \frac{\varepsilon\delta}{3}\xi\left(\frac{\partial G(\xi,0)}{\partial \eta}\right)^3 \quad (22b)$$

The mass transfer rate, Sh_x is defined as,

$$Sh_x = -\frac{1}{\sqrt{2}} Gr_x^{1/4} \frac{\partial \phi(\xi,0)}{\partial \eta} \quad (23)$$

To provide a benchmark for numerical solutions, a number of special cases of the general flow model can be retrieved from Eqs. (13)–(16) with conditions (17a,b). With $Fs \to 0$, inertial effects disappear and only a bulk porous matrix resistance (Darcian) acts on the partially-ionized fluid in the porous medium. With $Da \to \infty$, the regime permeability becomes infinite and the porous fibers vanish in the limit. The model contracts to purely fluid hydromagnetic convection flow. For the case of

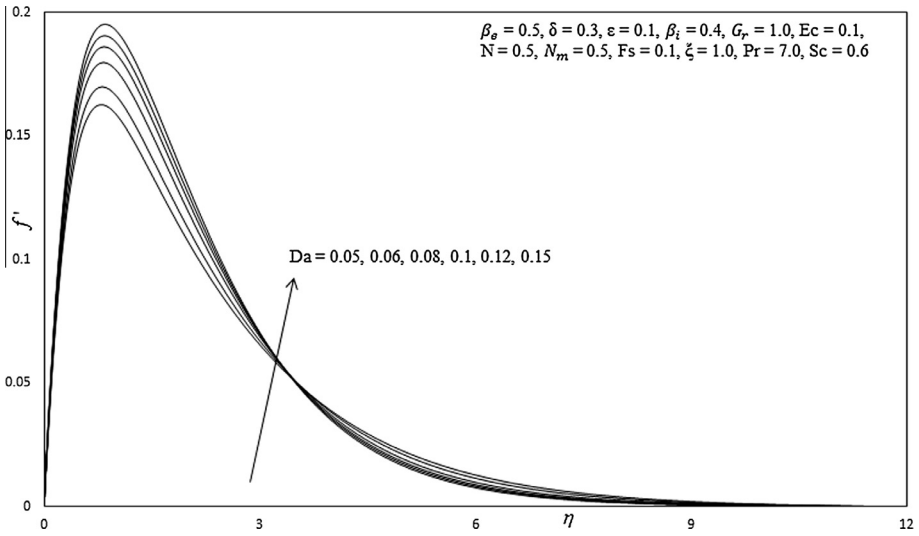

Figure 7a Influence of *Da* on primary velocity profiles.

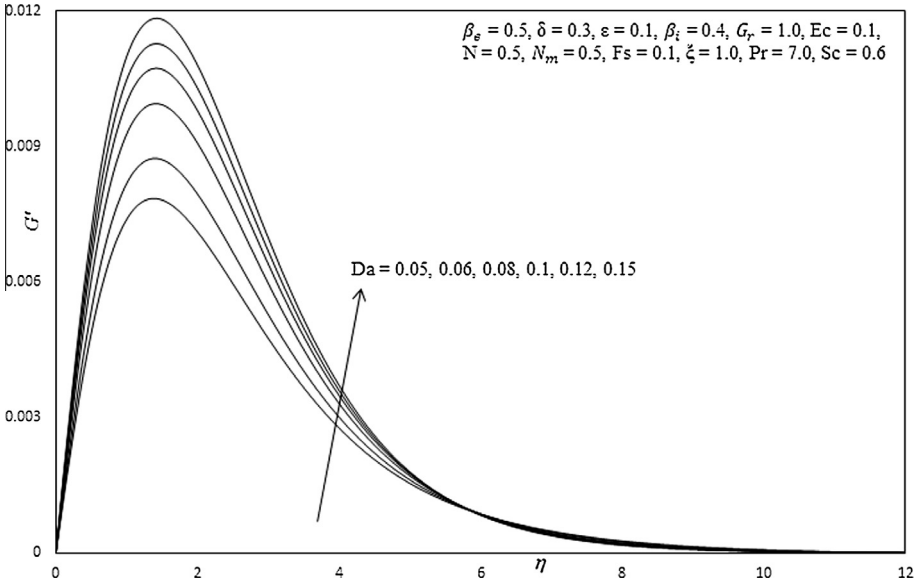

Figure 7b Influence of *Da* on secondary velocity profiles.

$Ec \to 0$, both viscous heating and Joule electric current heating terms vanish in the energy conservation equation. Finally, with absence of magnetic field effects, $N_m \to 0$, which also negates Hall current and ionslip effects in the momentum equations.

5. Keller Box computational solutions

The Keller-Box implicit difference method (**KBM**) is utilized to solve the nonlinear boundary value problem defined by Eqs. (13)–(16) with boundary conditions (17). Although other powerful numerical methods have been developed in fluid mechanics including differential transform quadrature [22] and MAPLE shooting methods [48], for *parabolic* problems (of which boundary layer flows are an excellent example), Keller's box technique [49] remains extremely popular since it easily solves two-coordinate problems (partial differential families of equations). Although Keller's box scheme was developed over four decades ago, it has witnessed a recent re-surge in implementation. Recent areas in which this scheme has been employed include Jeffrey's fluid [50–51], tangent hyperbolic fluid [52], magnetohydrodynamics [53], wavy surface convection flows [54], nanofluids [55] and drainage sheet flows [56]. The Keller-Box discretization is *fully coupled* at each step which reflects the physics of parabolic systems – which are also fully coupled. Discrete calculus associated with the Keller-Box scheme has also been shown to be fundamentally different from all other mimetic (physics capturing) numerical methods, as elaborated by Keller [49]. The Keller Box Scheme comprises four stages:

(1) Decomposition of the *N*th order partial differential equation system to *N* first order equations.
(2) Finite Difference Discretization.

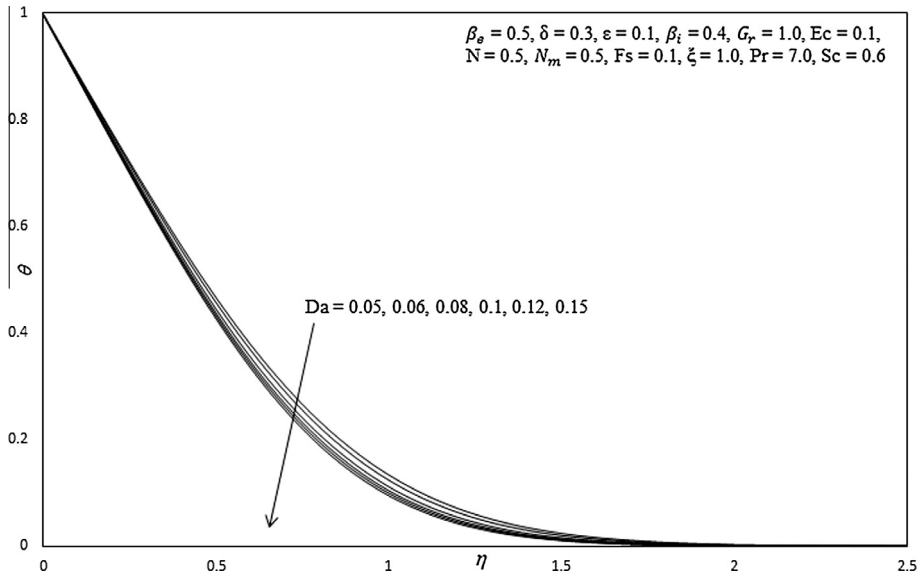

Figure 7c Influence of *Da* on temperature profiles.

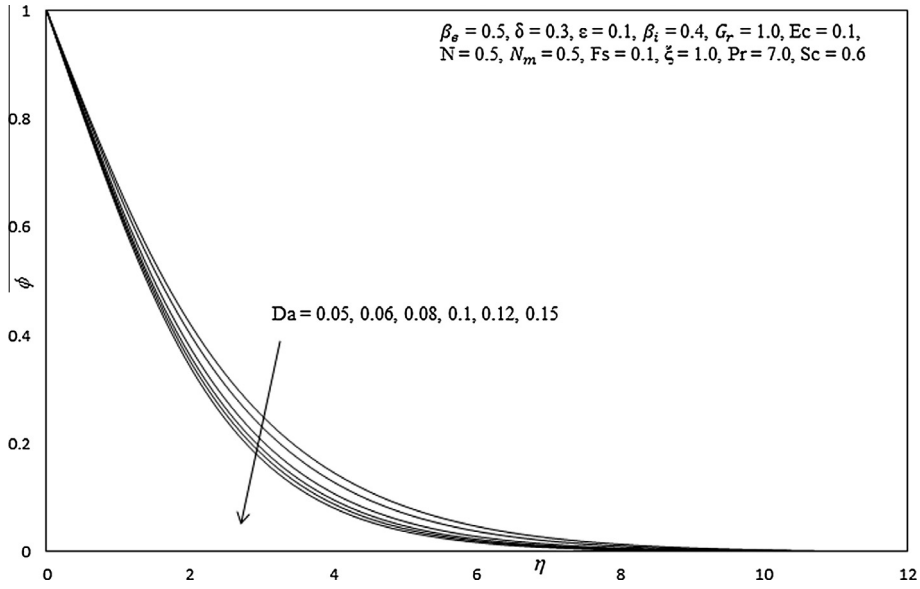

Figure 7d Influence of *Da* on concentration profiles.

(3) Quasilinearization of Non-Linear Keller Algebraic Equations.
(4) Block-tridiagonal elimination solution of the Linearized Keller Algebraic Equations.

6. Keller box computational results and discussion

Comprehensive solutions have been obtained and are presented in Tables 1–4 and Figs. 2–15. The numerical problem comprises two independent variables (ξ, η), four dependent fluid dynamic variables (f, G, θ, ϕ) and different thermophysical and body force control parameters, namely, ε, δ, β_e, β_i, N_m, Pr, Da, Fs, Gr, Ec. The following default parameter values i.e. $\varepsilon = 0.1$, $\delta = 0.3$, $\beta_e = 0.5$, $\beta_i = 0.4$, $N_m = 0.5$, $Pr = 7.0$, $Gr = 1.0$, $Ec = Da = Fs = 0.1$ are prescribed (unless otherwise stated). Validation with Nakamura's tridiagonal finite difference method (**NTM**) [57] is provided in the next section with Tables 5 and 6.

7. Validation with Nakamura tridiagonal method (NTM)

To validate the present solutions, we have also utilized an efficient finite difference procedure of the implicit type, originally developed by Nakamura [58] to solve the ninth order nonlinear partial differential boundary value problem defined by Eqs. (13)–(16) under boundary conditions (17a,b). As with other difference schemes, a reduction of the higher order differential

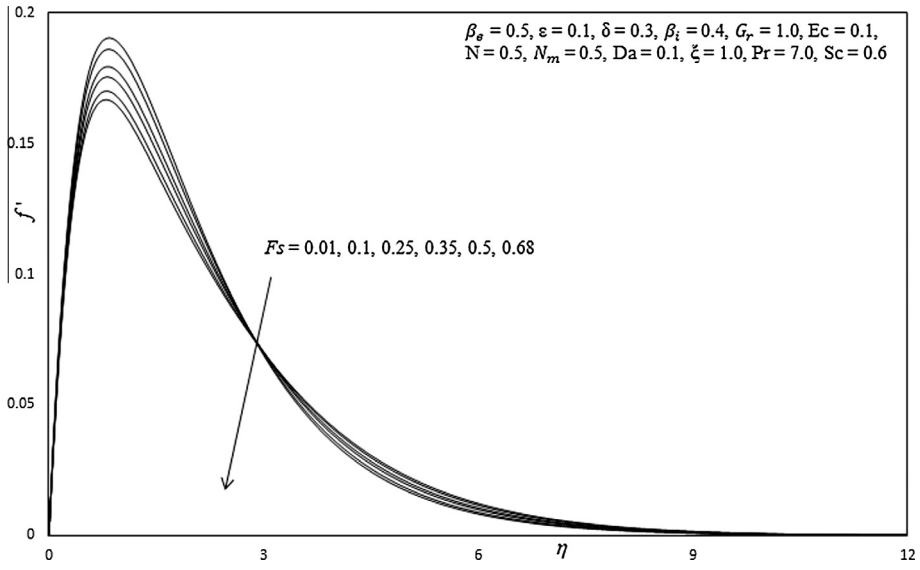

Figure 8a Influence of *Fs* on primary velocity profiles.

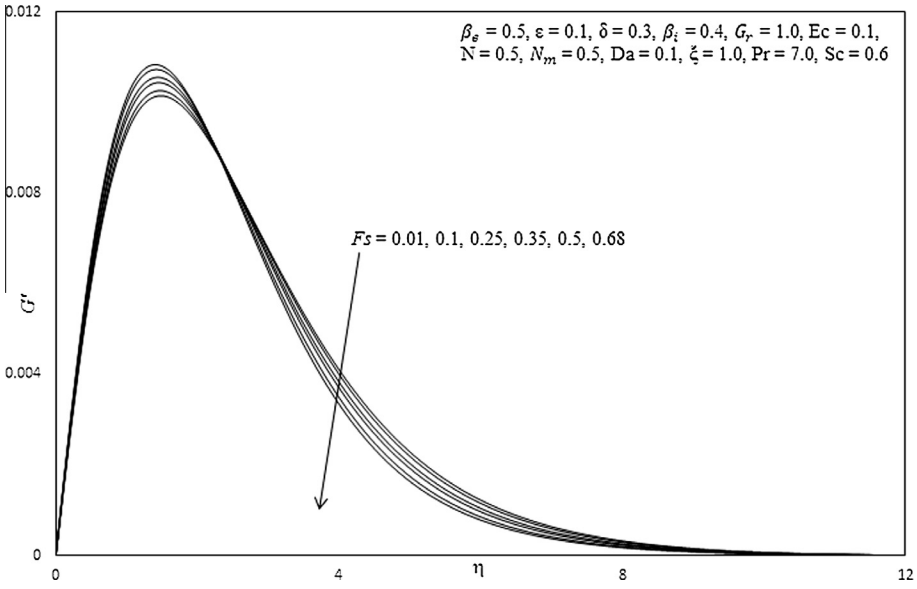

Figure 8b Influence of *Fs* on secondary velocity profiles.

equations arising is intrinsic also to the Nakamura tridiagonal method (**NTM**). **NTM** is also particularly accurate at simulating parabolic problems as exemplified by boundary layer flows. Applications of **NTM** in micromorphic and other non-Newtonian flows include flat plate micropolar convection [59], Ostwald–deWaele shear-thinning plume flows [60], centrifugal heart pump hemodynamics [61], and viscoelastic biopolymer wedge flows [62]. More recently NTM has been successfully utilized in studying nanofluid biconvection of oxytactic micro-organisms in a microbial porous media fuel cell by Anwar Bég et al. [63] and micropolar conducting biopolymer enrobing flows [64]. **NTM** works well for both one-dimensional (ordinary differential equation systems) and two-dimensional (partial differential) non-similar flows. **NTM** entails a combination of the following aspects. In the computations both an inner loop and outer loop are required, the former to advance the solution in the η-direction, and the latter to advance it in the ξ-direction. The flow domain is discretized using an equi-spaced finite difference mesh in the (ξ, η)-directions. The partial derivatives for F, G, H with respect to ξ, η are evaluated by central difference approximations. A double iteration loop based on the method of successive substitution is employed. The finite difference discretized equations are solved as a *linear* second order boundary value problem on the ξ, η-domain. All the conservation equations, except the primary momentum Eq. (13) are *second order* equations, and for these Eqs., viz (14)–(16) only a *direct* substitution is needed. Setting:

$$P = f' \tag{24}$$

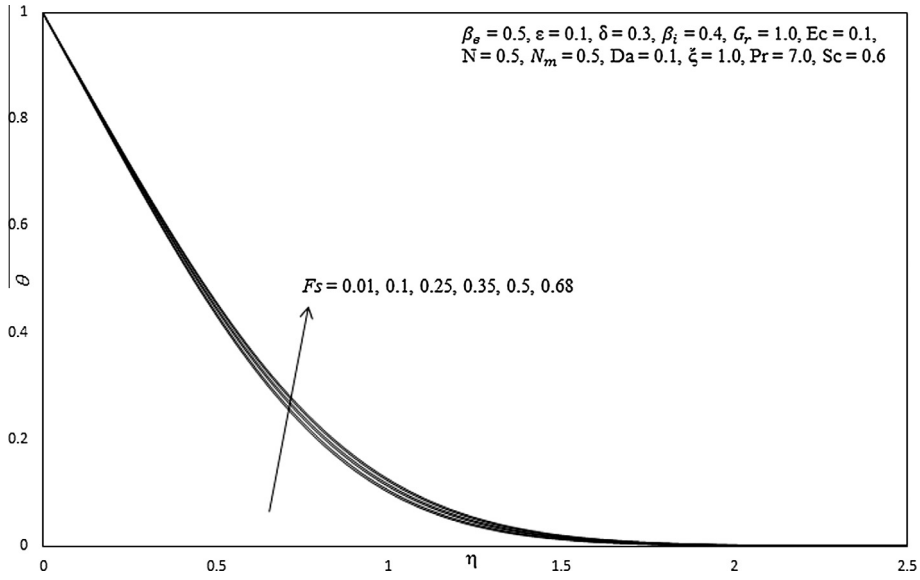

Figure 8c Influence of *Fs* on temperature profiles.

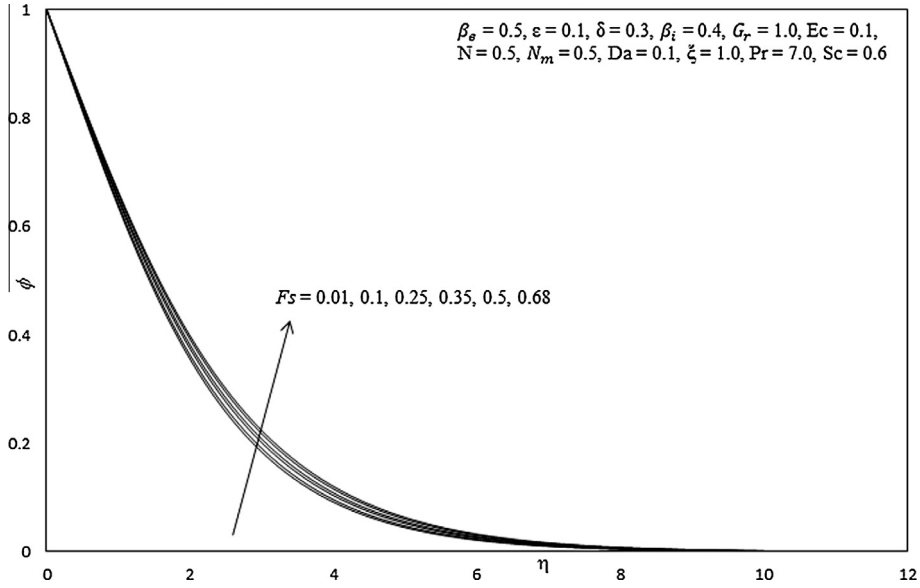

Figure 8d Influence of *Fs* on concentration profiles.

$$Q = G \tag{25}$$

$$R = \theta \tag{26}$$

$$H = \phi \tag{27}$$

Eqs. (13)–(16) then assume the following form:

Nakamura primary momentum equation:

$$A_1 P'' + B_1 P' + C_1 P = S_1 \tag{28}$$

Nakamura secondary momentum equation:

$$A_2 Q'' + B_2 Q' + C_2 Q = S_2 \tag{29}$$

Nakamura energy equation:

$$A_3 R'' + B_3 R' + C_3 R = S_3 \tag{30}$$

Nakamura mass equation:

$$A_4 H'' + B_4 H' + C_4 H = S_4 \tag{31}$$

where $A_{i=1\ldots4}$, $B_{i=1\ldots4}$, $C_{i=1\ldots4}$ are the *Nakamura matrix coefficients*, $S_{i=1\ldots4}$ are the *Nakamura source terms* containing a mixture of variables and derivatives associated with the variables (omitted for brevity). The Nakamura Eqs. (29)–(31) are transformed to finite difference equations and these are orchestrated to form a tridiagonal system which is solved iteratively. Tables 5 and 6 document the comparison

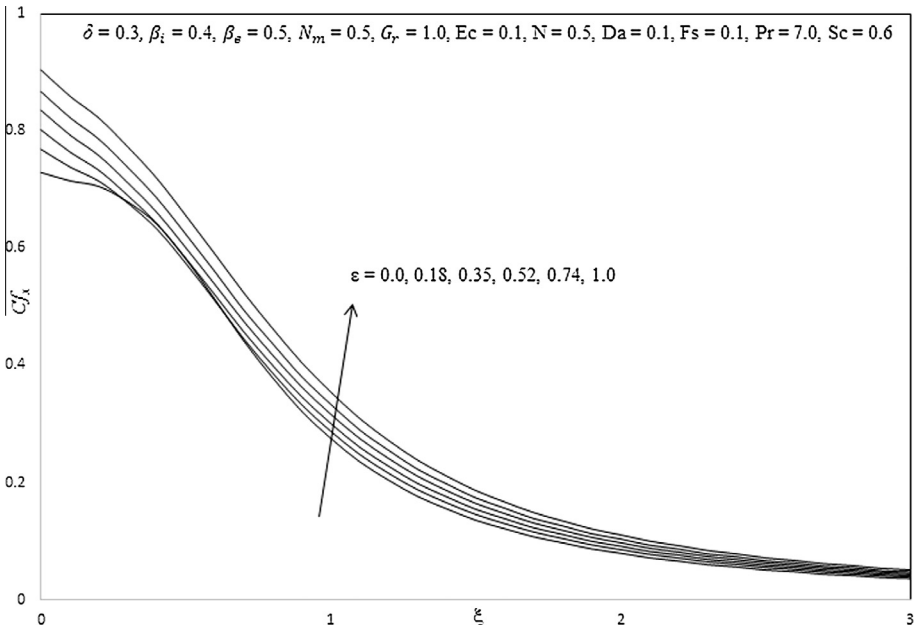

Figure 9a Influence of ε on skin friction coefficient.

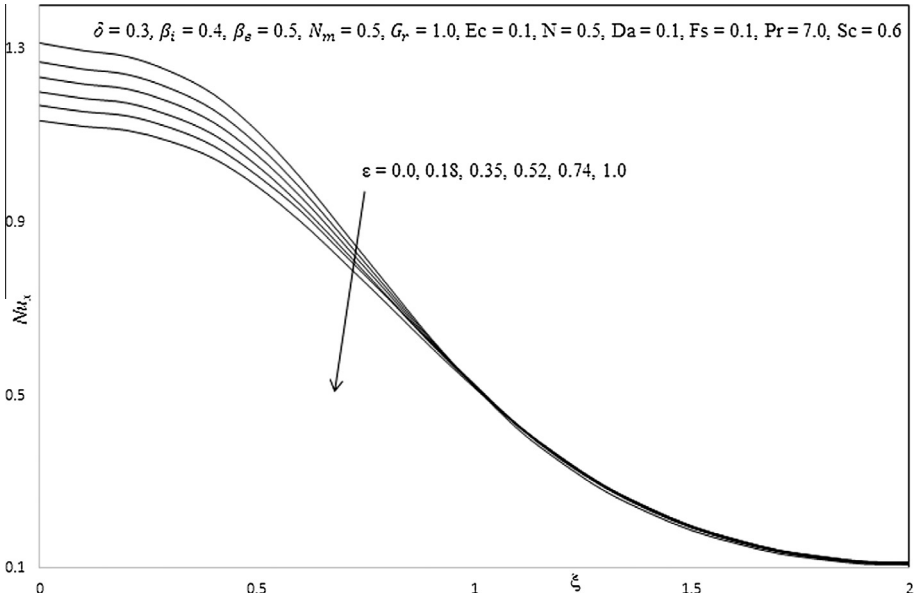

Figure 9b Influence of ε on Nusselt number.

of **KBM** and **NTM** solutions for the effects of Hall current parameter (β_e) and ionslip parameter (β_i) in addition to ξ-coordinate on *primary shear stress function*, *secondary shear stress function and heat transfer rate*. Excellent agreement is achieved. Confidence in the Keller-box solutions is therefore high.

8. Discussion

Figs. 2a–2d depict the primary velocity (f'), secondary velocity (G), temperature (θ) and concentration (ϕ) distributions with increasing Eyring–Powell fluid parameter, ε. Very little tangible effect is observed in Figs. 2a and 2b, although there is a very slight decrease in primary and secondary velocities with increase in ε. Conversely, there is only a very slight increase in temperature and concentration magnitudes in Figs. 2c and 2d with a rise in ε. The mathematical model reduces to the *Newtonian viscous flow model* as $\varepsilon \to 0$ and $\delta \to 0$. The momentum boundary layer equations in this case contract to the familiar equation for *Newtonian mixed convection* from a vertical surface, viz.

$$f''' + 3ff'' - 2f'^2 + (\theta + N\phi) - \frac{2}{Da\,Gr_x^{1/2}}\xi^4 f' - \frac{4Fs}{Da}\xi^2 f'^2 - \frac{2Nm}{[\alpha_e^2 + \beta_e^2]}\xi[\alpha_e f' + \beta_e G] = 2\xi\left[f'\frac{\partial f'}{\partial \xi} - f''\frac{\partial f}{\partial \xi}\right]$$

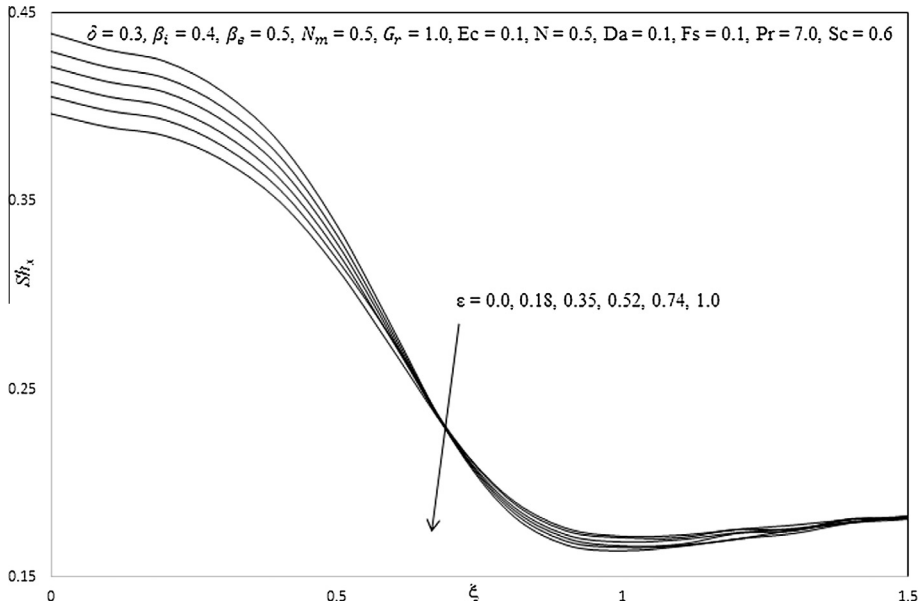

Figure 9c Influence of ε on Sherwood number.

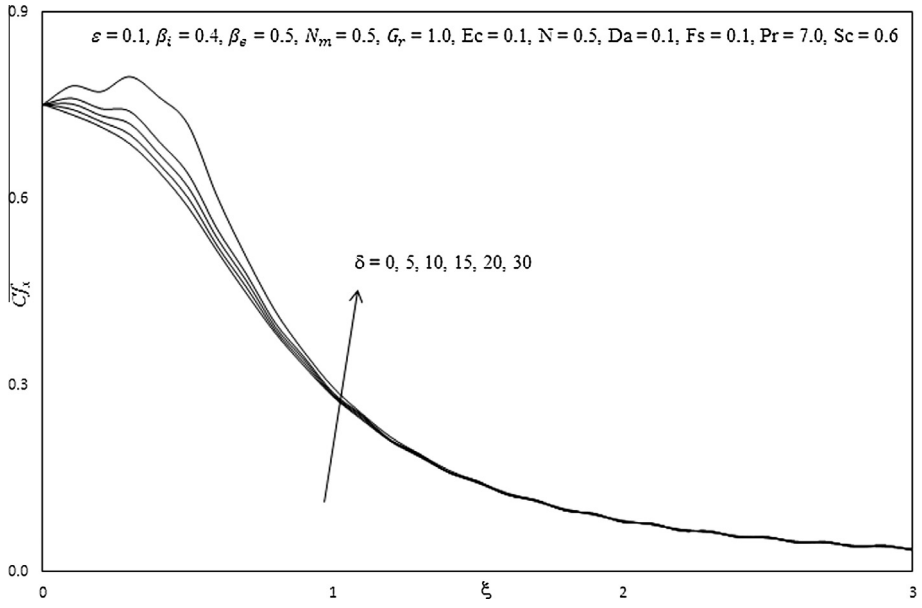

Figure 10a Influence of δ on skin friction coefficient.

and

$$G'' + 3fG' - 2Gf' - \frac{2}{Da\,Gr_x^{1/2}}\xi^4 G - \frac{4Fs}{Da}\xi^2 G^2 - \frac{2Nm}{[\alpha_e^2+\beta_e^2]}\xi[\alpha_e f' + \beta_e G] = 2\xi\left[f'\frac{\partial f'}{\partial \xi} - f''\frac{\partial f}{\partial \xi}\right]$$

The thermal boundary layer Eq. (10) and the mass conservation Eq. (11) remain unchanged.

Figs. 3a–3d illustrate the effect of the increasing local non-Newtonian fluid parameter, δ, primary velocity (f'), secondary velocity (G), temperature (θ) and concentration (ϕ) distributions through the boundary layer regime. Very little tangible effect is observed in Fig. 3a, although there is a very slight increase in primary and secondary velocity with increase in δ. Conversely, temperature and concentration are consistently reduced with increasing values of δ.

Figs. 4a–4d, depict the evolution of primary velocity (f'), secondary velocity (G), temperature (θ) and concentration (ϕ) functions with a variation in Hall current parameter, β_e. This parameter generates the cross flow effect in Magnetohydrodynamics. The Hall current parameter arises in both the primary and secondary momentum Eqs. (13) and (14) via the *cross-flow* coupling terms, $-\frac{2N_m}{[\alpha_e^2+\beta_e^2]}\xi[\alpha_e f' + \beta_e G]$ and $-\frac{2N_m}{[\alpha_e^2+\beta_e^2]}\xi[\alpha_e G - \beta_e f']$. It arises in quadratic form as a denominator i.e. $-\frac{2N_m}{[\alpha_e^2+\beta_e^2]}$ in both and is coupled to the secondary velocity, G, in the former,

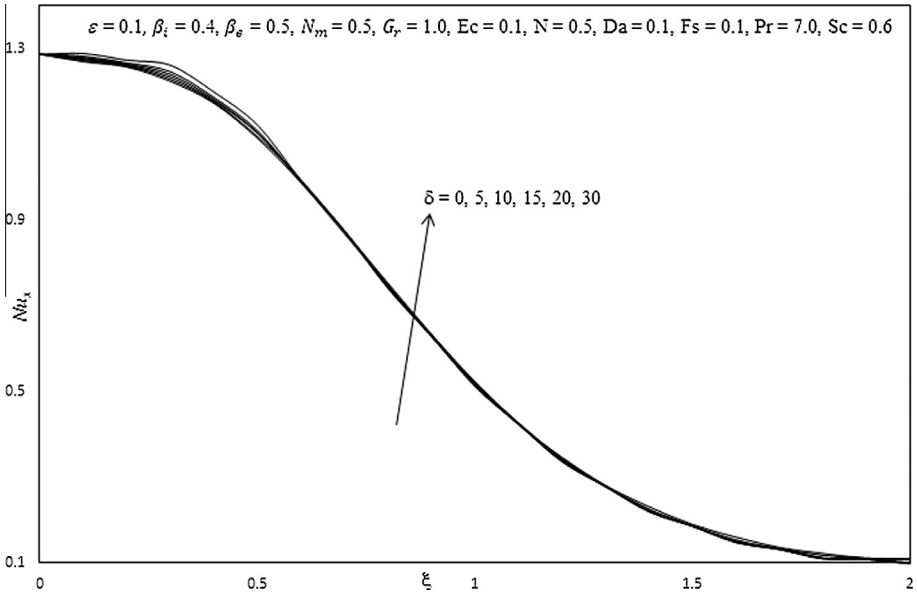

Figure 10b Influence of δ on Nusselt number.

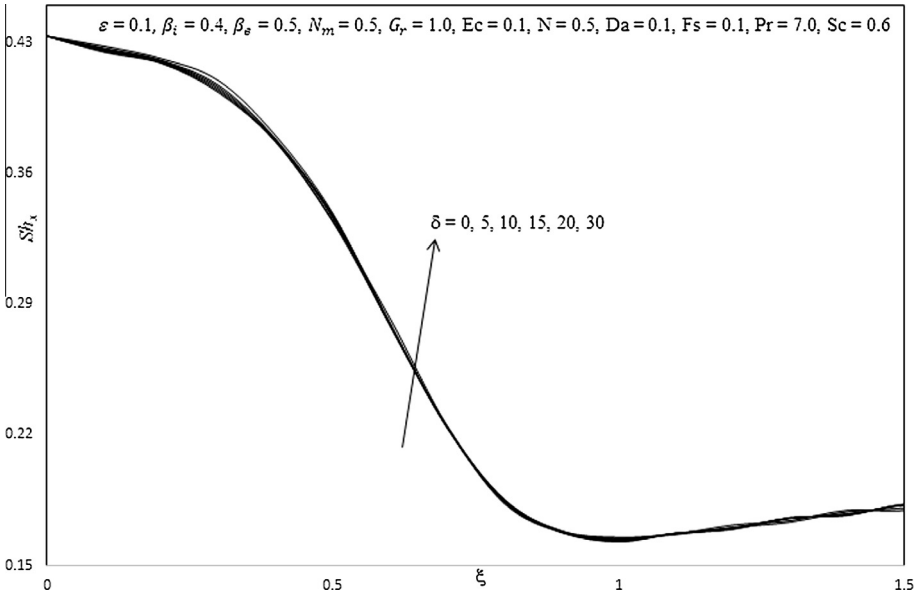

Figure 10c Influence of δ on Sherwood number.

and to the primary velocity, f' in the latter. The effect is for acceleration in the primary flow with greater Hall current parameter, as observed in Fig. 4a. The peak velocity is attained some distance from the plate surface. The primary velocity profiles in all cases converge asymptotically to vanishing free stream velocity, demonstrating that a sufficiently large infinity is prescribed in the computations. Momentum supplied to accelerate the primary flow is depleted from the secondary flow and this manifests in a strong deceleration in secondary velocity, as shown in Fig. 4b. With increasing Hall parameter, the peak secondary velocity is displaced closer to the plate surface. This does not occur for the primary velocity. A weak reduction in temperatures accompanies an increase in Hall parameter (Fig. 4c), which is attributable to the inverse square effect arising in the Joule heating term in Eq. (15), viz $+\frac{2N_m Ec}{[\alpha_e^2+\beta_e^2]}\xi^3[f'^2+G^2]$ – this term couples the primary and secondary velocity fields to the energy field. For non-zero Eckert number, this term has a non-trivial effect on the temperature distribution. With greater Hall parameter the thermal boundary layer is cooled and thickness is decreased. Also a decrease in concentration is observed in Fig. 4d for increasing values of Hall parameter.

Figs. 5a–5d illustrate the effect of the ionslip parameter i.e. β_i on the primary velocity (f'), secondary velocity (G), temperature (θ) and concentration (ϕ) distributions through the boundary layer regime. Primary velocity is enhanced with increasing β_i (Fig. 5a). Conversely, secondary velocity, temperature and concentration are depressed with increasing β_i values (Figs. 5b–5d respectively). Ionslip arises in the parameter,

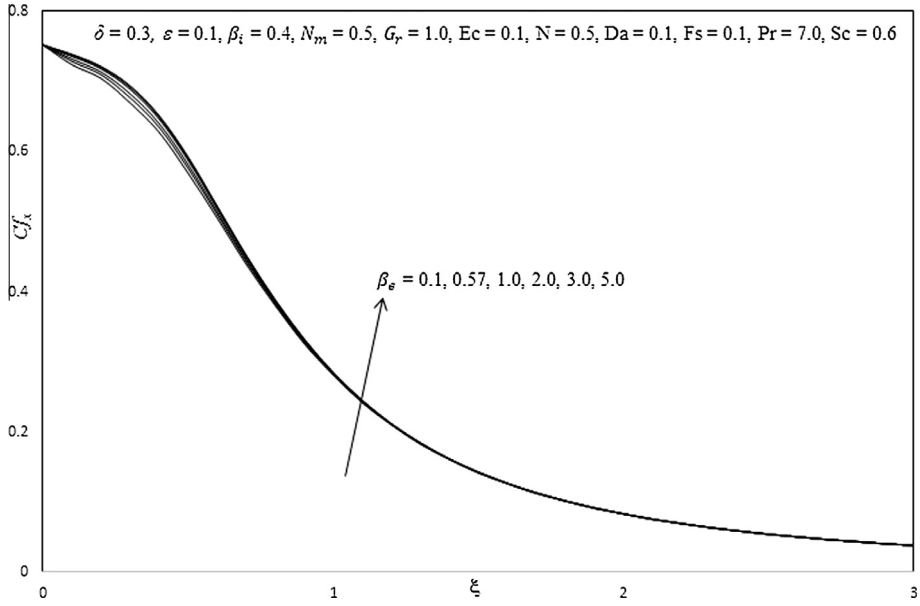

Figure 11a Influence of β_e on skin friction coefficient.

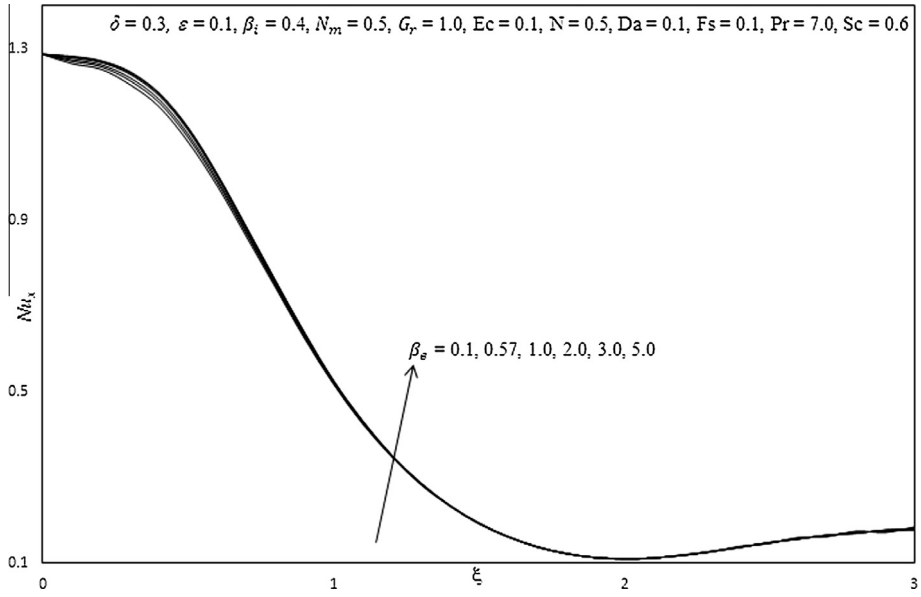

Figure 11b Influence of β_e on Nusselt number.

$\alpha_e = 1 + \beta_i \beta e$, which causes a heating effect as the ions slip in the magnetic field and a deceleration in the secondary flow. Only primary flow is positively influenced by the ionslip effect, and this characteristic is beneficial in MHD energy generator systems. It is also noteworthy to mention that generally values of primary velocity are several orders of magnitude greater than secondary velocity, a familiar phenomenon in MHD flows. Similar effects have been reported by other authors, although in the absence of non-isothermal plate conditions.

Figs. 6a–6d present the distribution of primary velocity (f'), secondary velocity (G), temperature (θ) and concentration (ϕ) functions for various values of the magnetic body force parameter i.e. Hartmann number, $N_m = \frac{\sigma B_o^2 L^{1/2}}{2\rho v C^2}$. An increase in N_m, strongly decelerates the flow i.e., reduces primary velocity values. In all profiles a peak arises near the surface of the plate and this peak is displaced progressively closer to the wall with an elevation in N_m values. This migration phenomenon has been reported by many other researchers [11]. Essentially a greater retarding effect is generated in the flow with greater N_m values (i.e., stronger magnetic field strengths), which causes the prominent depression in velocities. For $N_m = 1$ the magnetic Lorentzian drag force will be of the same order of magnitude as the viscous hydrodynamic force. For $N_m > 1$, hydromagnetic drag will dominate and vice versa for $N_m < 1$. Therefore, in near-wall flows of magnetohydrodynamic generators or indeed materials processing, the flow

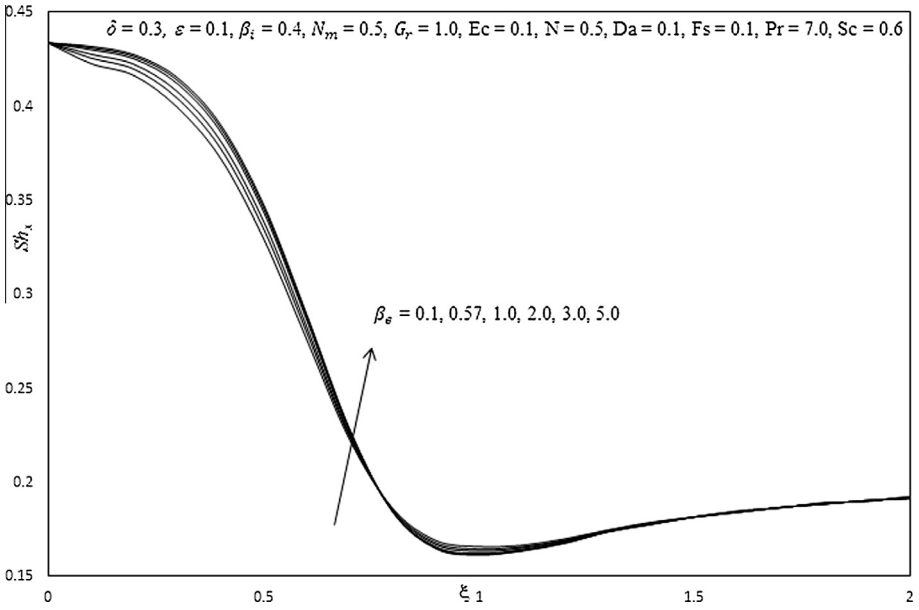

Figure 11c Influence of β_e on Sherwood number.

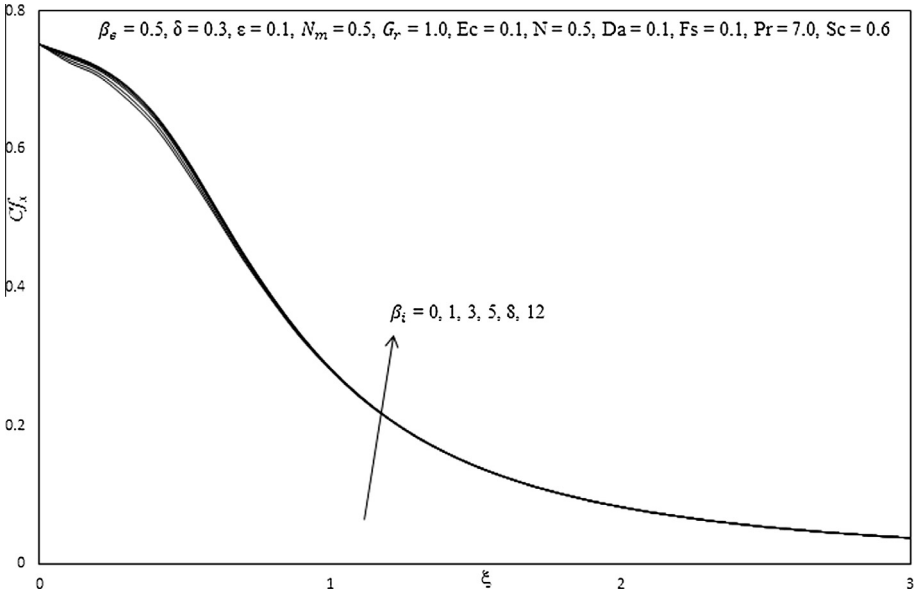

Figure 12a Influence of β_i on skin friction coefficient.

can be very effectively controlled with a magnetic field. However, increasing N_m is found to accelerate the secondary velocity, temperature and concentration. The secondary flow acceleration is beneficial in certain manipulation processes in MHD materials technology as it encourages a more homogenous constitution in materials. The increase in temperature is generated by the dissipation in supplementary work expended in dragging the fluid against the action of the magnetic field. This work is converted to thermal energy which heats the fluid and enhances thermal boundary layer thickness.

Figs. 7a–7d depict the response of primary velocity (f'), secondary velocity (G), temperature (θ) and concentration (ϕ) to a variation in the Darcy parameter, Da. Primary and secondary velocities are clearly enhanced considerably with increasing Da as shown in Figs. 7a and 7b, since greater permeability of the regime corresponds to a decrease in Darcian drag force. The velocity peaks close to the plate surface are also found to be displaced further from the wall with increasing Darcy number. Porous media with greater permeability therefore assist both primary and secondary flow development whereas smaller permeability manifests in greater solid matrix impedance and decelerates both flow fields. A very strong decrease in temperature and concentration, as shown in Figs. 7c and 7d, occurs with increasing Da values. The progressive reduction in solid fibers in the porous medium with large Da values serves to decrease thermal conduction heat transfer in the regime. This inhibits the diffusion of thermal energy from the plate surface to the regime and cools the boundary layer also decreasing

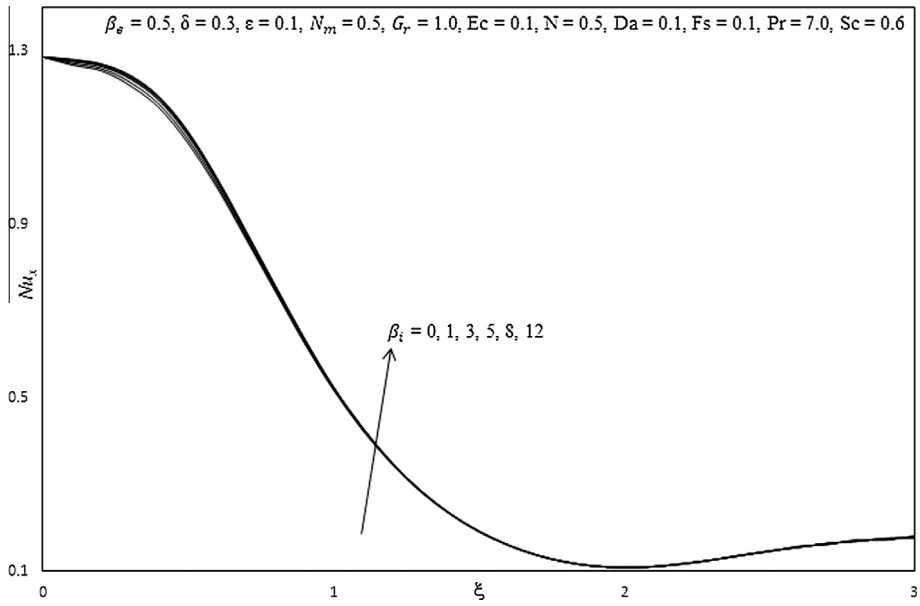

Figure 12b Influence of β_i on Nusselt number.

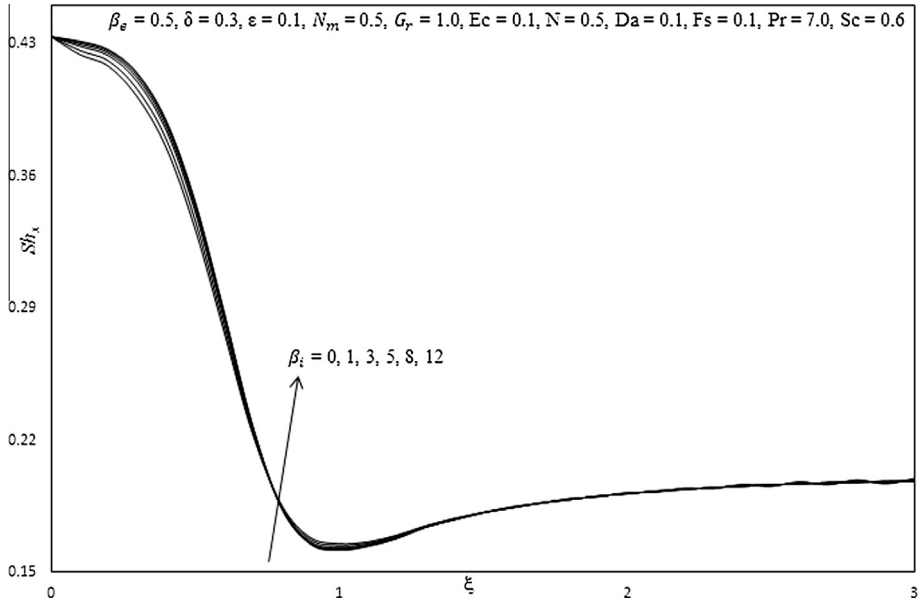

Figure 12c Influence of β_i on Sherwood number.

thermal boundary layer thickness. The presence of a porous medium therefore induces a significant effect on momentum and thermal diffusion in the system and provides a good mechanism for thermal regulation and flow control.

Figs. 8a–8d present the typical profiles for velocity functions, temperature and concentration distribution for various values of Forchheimer parameter, *Fs*. An increase in *Fs* markedly *decelerates* the flow as illustrated in Figs. 8a and 8b, for some considerable distance in the boundary layer, transverse to the plate surface. Inertial quadratic drag has a stronger effect closer to the wall. Forchheimer drag however is second order and the increase in this "form" drag effectively swamps the momentum development, thereby decelerating the flow, in particular near the plate surface. The term "non-Darcian" does not allude to a different regime of flow, but to the *amplified* effects of Forchheimer drag at higher velocities, as elaborated also in Anwar Bég et al. [65] and Prasad et al. [55]. With a significant increase in *Fs* there is also a slight elevation in temperatures and concentrations (Figs. 8c and 8d) in the regime. Thermal boundary layer thickness is therefore weakly enhanced with greater Forchheimer effect.

Figs. 9a–9c show the influence of Eyring–Powell fluid parameter, ε on dimensionless skin friction coefficient, heat and mass transfer rates. It is observed that the dimensionless skin friction is increased with the increase in ε i.e. the boundary layer flow is accelerated with decreasing viscosity effects in the

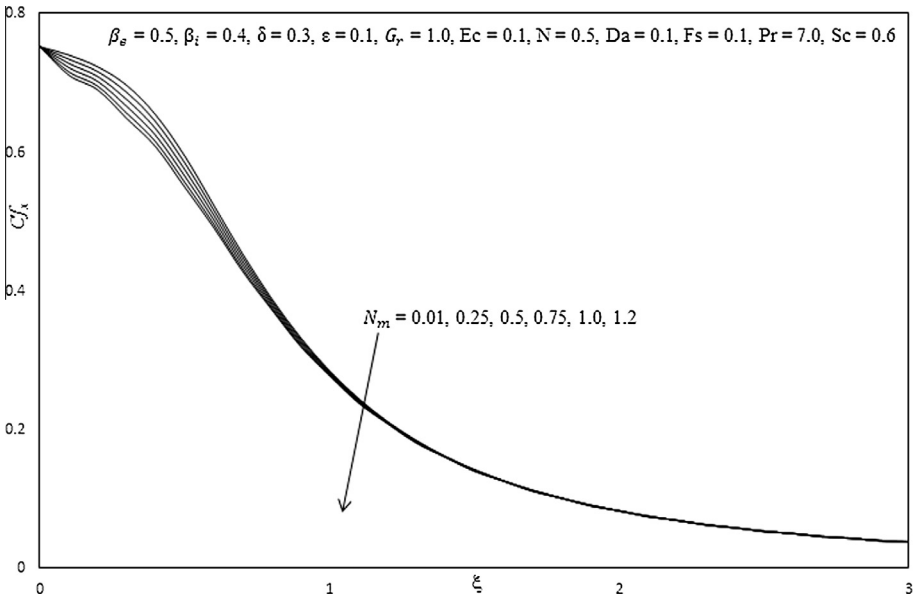

Figure 13a Influence of N_m on skin friction coefficient.

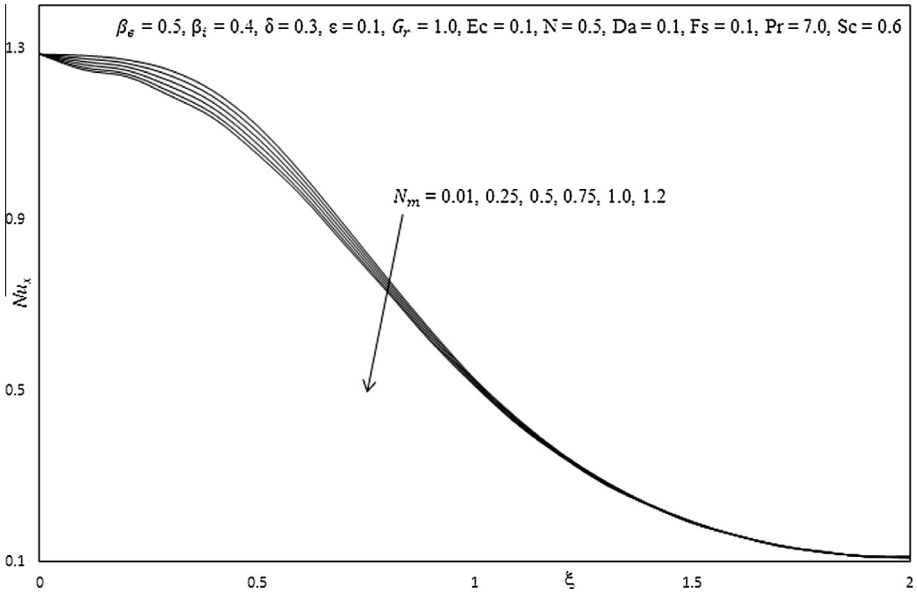

Figure 13b Influence of N_m on Nusselt number.

non-Newtonian regime. Conversely, the surface heat and mass transfer rates are substantially *decreased* with increasing ε values. Decreasing viscosity of the fluid (induced by increasing the ε value) reduces thermal diffusion as compared with momentum diffusion.

Figs. 10a–10c illustrate the influence of the local non-Newtonian parameter, δ, on the dimensionless skin friction coefficient, heat and mass transfer rate. The skin friction (Fig. 10a) is accentuated with increasing δ, however only for very large values of the transverse coordinate, ξ. The flow is therefore strongly accelerated along the vertical surface far from the lower stagnation point. Heat and mass transfer rates are also enhanced with increasing δ, *again at large values of* ξ, as computed in Figs. 10b and 10c.

Figs. 11a–11c present the influence of increasing hall current parameter (β_e) on the dimensionless skin friction coefficient, heat and mass transfer rate, along with a variation in transverse coordinate (ξ). With an increase in β_e, the skin friction, heat and mass transfer rate are also found to increase.

Figs. 12a–12c show the influence of increasing ionslip parameter (β_i) on the dimensionless skin friction coefficient, heat and mass transfer rate along with a variation in transverse coordinate (ξ). With the increasing β_i, a very slight increase is observed in the dimensionless skin friction coefficient, heat and mass transfer rate.

Figs. 13a–13c present the influence of increasing Hartmann (magnetic body force) number (N_m) on the dimensionless skin friction coefficient, heat and mass transfer rate, along with a

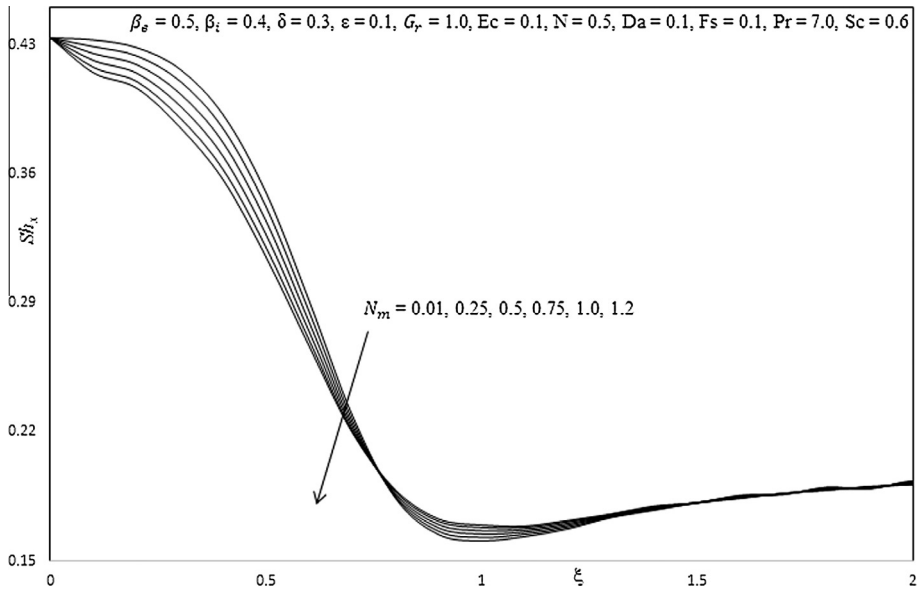

Figure 13c Influence of N_m on Sherwood number.

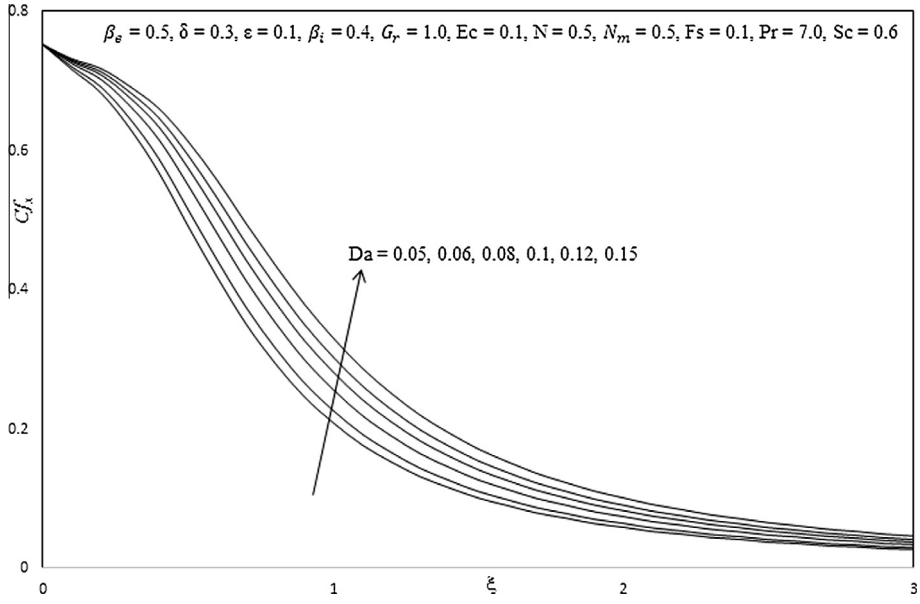

Figure 14a Influence of *Da* on skin friction coefficient.

variation in transverse coordinate (ξ). It is observed that increasing N_m, decreases the dimensionless skin friction coefficient, heat and mass transfer rate. This verifies earlier computations described showing that the flow is retarded with magnetic field but the fluid is heated. The transport of heat from the fluid to the plate corresponds to greater heat transfer rates and a drop in fluid temperature.

Figs. 14a–14c document the effect of increasing Darcy number (*Da*) on the dimensionless skin friction coefficient, heat and mass transfer rate, along with a variation in transverse coordinate (ξ). Increasing *Da*, is found to elevate the dimensionless skin friction coefficient, heat and mass transfer rate.

Figs. 15a–15c document the effect of increasing Forchheimer quadratic drag number (*Fs*) on the dimensionless skin friction coefficient, heat and mass transfer rate, along with a variation in transverse coordinate (ξ). Increasing *Fs,* is found to decrease the dimensionless skin friction coefficient, heat and mass transfer rate.

Table 1 presents the influence of increasing Eyring–Powell fluid parameter (ε), Hall current parameter (β_e) and ionslip parameter (β_i) on skin friction coefficient, heat transfer rate and mass transfer rate, along with a variation in transverse coordinate (ξ). Increasing ε, increases the skin friction coefficient, whereas, decreases heat transfer rate and mass transfer rate. An increasing β_e, is found to increase skin friction coeffi-

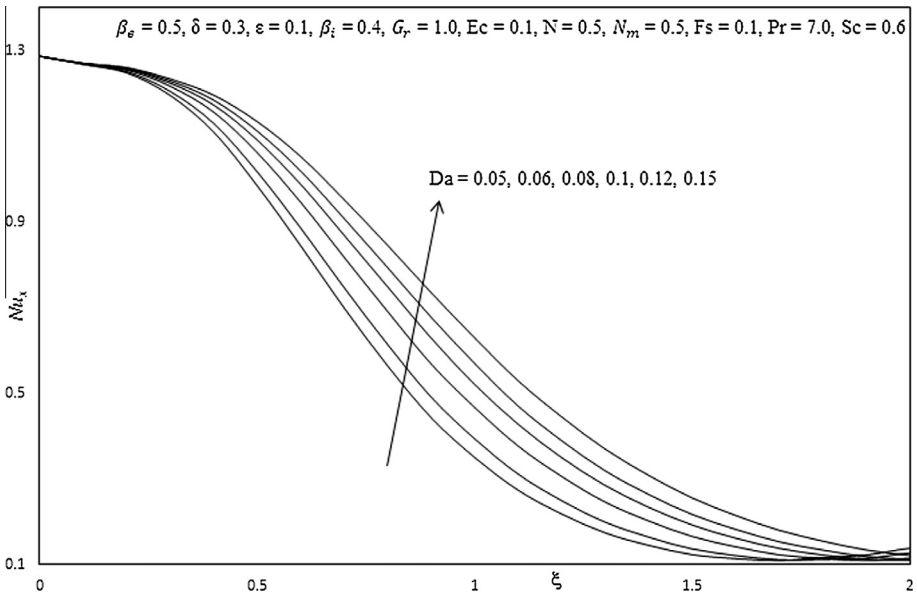

Figure 14b Influence of *Da* on Nusselt number.

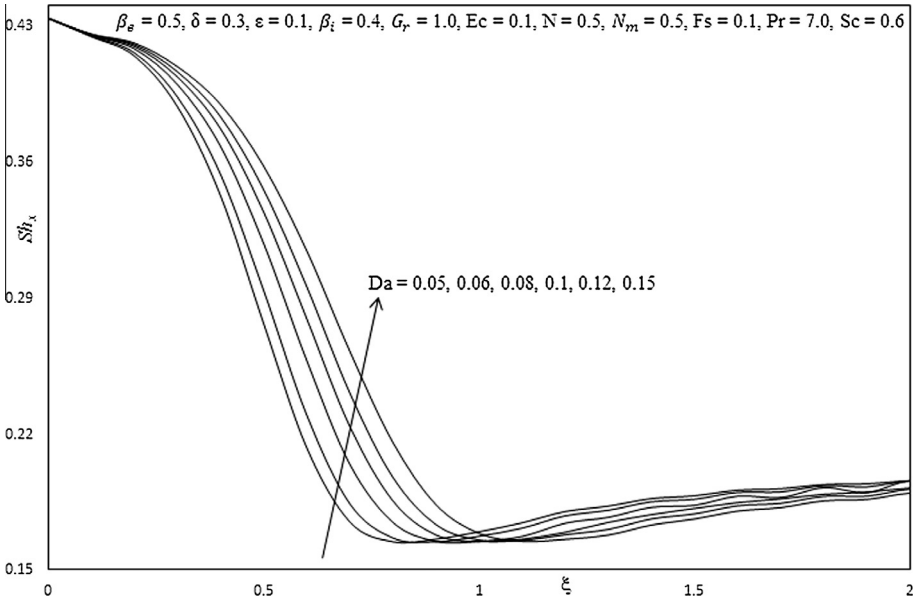

Figure 14c Influence of *Da* on Sherwood number.

cient, heat transfer rate and mass transfer rate. Increasing β_i, is observed to increase the skin friction coefficient, heat transfer rate and mass transfer rate.

Table 2 presents the influence of increasing Schmidt number (*Sc*) and Prandtl number (*Pr*) on skin friction coefficient, heat transfer rate and mass transfer rate along with a variation in transverse coordinate (ξ). It is observed that the skin friction coefficient is decreased slightly with increasing *Sc*. The heat transfer rate is reduced with increasing values of *Sc* but mass transfer rate is enhanced with increasing *Sc*. Increasing *Pr* is found to decrease the skin friction coefficient and mass transfer rate whereas the heat transfer rate is enhanced.

Table 3 documents the effect of increasing local non-Newtonian parameter based on length scale (δ), Forchheimer quadratic drag number (*Fs*) and Hartmann (magnetic body force) number (N_m) on skin friction coefficient, heat transfer rate and mass transfer rate, along with a variation in transverse coordinate (ξ). Increasing δ is found to increase skin friction coefficient, heat transfer rate and mass transfer rate. Conversely, increasing N_m decreases skin friction coefficient, heat transfer rate and mass transfer rate. The transport of heat from the fluid to the plate corresponds to greater heat transfer rates and a drop in fluid temperature. Also, increasing *Fs* is observed to decrease skin friction coefficient, heat transfer rate and mass transfer rate *Fs*.

Table 4 presents the influence of increasing Darcy parameter (*Da*) and Buoyancy ratio parameter (*N*) on skin friction coefficient, heat transfer rate and mass transfer rate, along

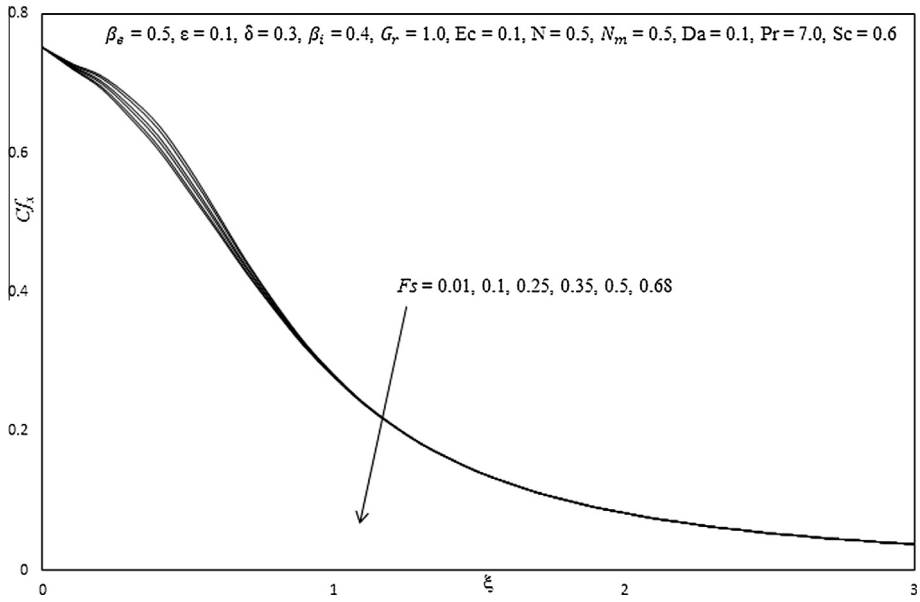

Figure 15a Influence of *Fs* on skin friction coefficient.

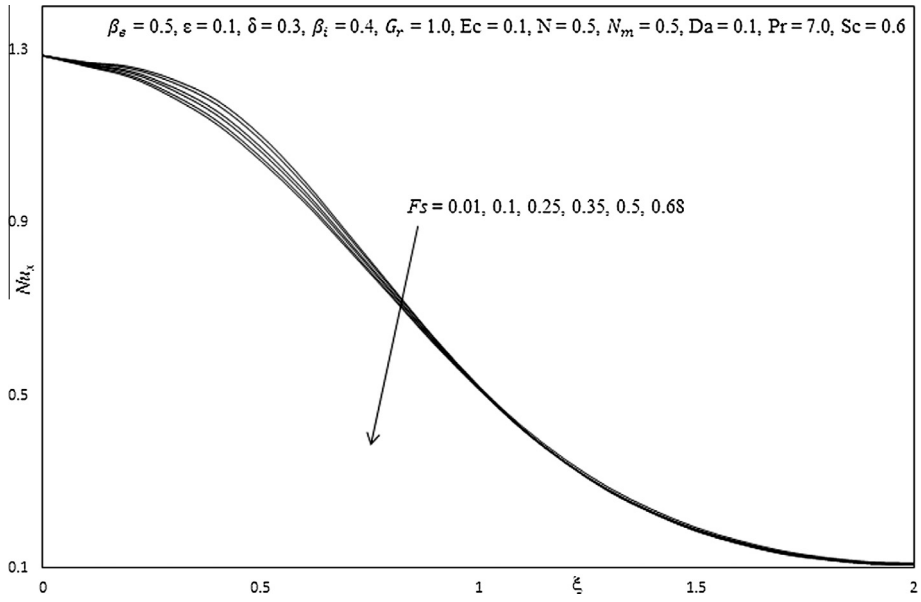

Figure 15b Influence of *Fs* on Nusselt number.

with a variation in transverse coordinate (ξ). It is observed that the skin friction coefficient, heat transfer rate and mass transfer rate are enhanced with increasing *Da*. It is also observed that increasing *N* increases the skin friction coefficient and heat transfer rate but decreases the mass transfer rate.

9. Conclusions

A mathematical model has been developed for the steady hydromagnetic free convection heat and mass transfer of non-Newtonian Eyring–Powell electrically-conducting fluid from a non-isothermal vertical surface adjacent to a non-Darcian porous medium in the presence of Hall currents, ion-slip currents and viscous and Joule heating effects. The boundary value problem (BVP) has been transformed from an (x, y, z) coordinate system to a (ξ, η) coordinate system. A number of important special cases have been described in addition to key engineering parameters being derived. The Keller box method has been employed to obtain implicit finite difference numerical solutions for the solution of the strongly coupled, nonlinear two-point boundary value problem. Extensive computations have been presented for the effects of *Eyring–Powell fluid parameter* (ε), *local non-Newtonian parameter based on length scale x* (δ), *Darcy number* (*Da*), *Forchheimer number* (*Fs*), *hydromagnetic parameter* (N_m), *Hall current parameter* (β_e), *ionslip parameter* (β_i), on the velocity fields and temperature distribution in the regime, with prescribed *Eckert number* (*Ec*), *Schmidt number* (*Sc*) and *Prandtl number* (*Pr*). Compu-

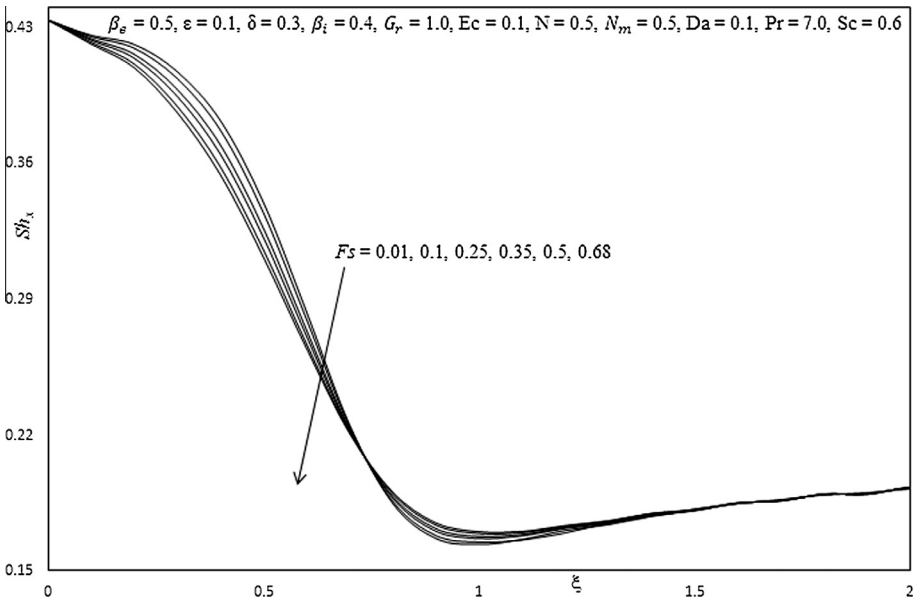

Figure 15c Influence of *Fs* on Sherwood number.

tations have been validated with Nakamura's tridiagonal difference method (NTM). A strong deceleration in primary and secondary flow has been shown to arise with greater non-isothermal effect at the wall, also leading to a decrease in temperatures. Increasing Hall parameter and ionslip are observed to accelerate weakly the primary flow but to strongly retard the secondary flow. Increasing Darcy number accelerates both primary and secondary flow but cools the fluid, as does an increase in Forchheimer number. The current study finds applications in both magnetic materials fabrication (e.g. liquid metal flows) and MHD energy generator near-wall flows. It also renders some useful benchmarks for more generalized commercial CFD simulations.

Acknowledgments

The authors are grateful to both reviewers and their comments which served to significantly improve the interpretative and other aspects of the present article.

References

[1] V. Ramachandra Prasad, A. Subba Rao, N. Bhaskar Reddy, B. Vasu, O. Anwar Bég, Modelling laminar transport phenomena in a Casson rheological fluid from a horizontal circular cylinder with partial slip, Proc. Inst. Mech. Eng., Part E: J. Process. Mech. Eng. 227 (4) (2013) 309–326.

[2] S. Abdul Gaffar, V. Ramachandra Prasad, E. Keshava Reddy, Magnetohydrodynamic free convection flow and heat transfer of non-Newtonian tangent hyperbolic fluid from horizontal circular cylinder with Biot number effects, Int. J. Appl. Comput. Math. (2016), http://dx.doi.org/10.1007/s40819-015-0130-y.

[3] S. Abdul Gaffar, V. Ramachandra Prasad, Bhuvana Vijaya, o. Anwar Beg, Mixed convection flow of magnetic viscoelastic polymer from a nonisothermal wedge with Biot number effects, Int. J. Eng. Math. 2015 (2015) 15, http://dx.doi.org/10.1155/2015/287623 Article ID 287623.

[4] S. Abdul Gaffar, V. Ramachandra Prasad, E. Keshava Reddy, O. Anwar Beg, Thermal radiation and heat generation/absorption effects on viscoelastic double-diffusive convection from an isothermal sphere in porous media, Ain Shams Eng. J. 5 (3) (2015) 1009–1030.

[5] N.S. Akbar, S. Nadeem, Rizwan Ul Haq, Sjiwei Ye, MHD stagnation point flow of Carreau fluid toward a permeable shrinking sheet: dual solutions, Ain Shams Eng. J. (2014), http://dx.doi.org/10.1016/j.asej.2014.05.006.

[6] N.S. Akbar, Z.H. Khan, R.U. Haq, S. Nadeem, Dual solutions in MHD stagnation-point flow of Prandtl fluid impinging on shrinking sheet, Appl. Math. Mech. 35 (7) (2014) 813–820.

[7] S. Nadeem, Rizwan Ul Haq, Noreen Sher Akbar, Z.H. Khan, MHD three-dimensional Casson fluid flow past a porous linearly stretching sheet, Alexandria Eng. J. 52 (4) (2013) 77–582.

[8] Noreen Sher Akbar, S. Nadeem, Rizwan Ul Haq, Z.H. Khan, Radiation effects on MHD stagnation point flow of nanofluid towards a stretching surface with convective boundary condition, Chin. J. Aeronaut. 26 (6) (2013) 1389–1397.

[9] Sohail Nadeem, Rizwan Ul Haq, Noreen Sher Akbar, MHD three-dimensional boundary layer flow of Casson nanofluid past a linearly stretching sheet with convective boundary condition, IEEE Trans. Nanotechnol. 13 (1) (2014) 109–115.

[10] Noreen Sher Akbar, S. Nadeem, Rizwan Ul Haq, Z.H. Khan, Numerical solutions of magnetohydrodynamic boundary layer flow of tangent hyperbolic fluid towards a stretching sheet, Indian J. Phys. 87 (11) (2013) 1121–1124.

[11] M.A. Hossain, Effect of Hall current on unsteady hydromagnetic free convection flow near an infinite vertical porous plate, J. Phys. Soc. (Japan) 55 (7) (1986) 2183–2190.

[12] T.L. Raju, V.V.R. Rao, Hall effects on temperature distribution in a rotating ionized hydromagnetic flow between parallel walls, Int. J. Eng. Sci. 31 (7) (1993) 1073–1091.

[13] E. Sawaya, N. Ghaddar, F. Chaaban, Evaluation of the Hall parameter of electrolyte solutions in thermosyphonic MHD flow, Int. J. Eng. Sci. 31 (7) (1993) 1073–1091.

[14] R. Bhargava, H.S. Takhar, Effect of Hall currents on the MHD flow and heat transfer of a second order fluid between two parallel porous plates, J. MHD, Plasma Space Res. 10 (2001) 73–87.

[15] K.R. Cramer, S.-I. Pai, Magnetofluid Dynamics for Engineers and Applied Physicists, McGraw-Hill, New York, USA, 1973.
[16] V.M. Soundalgekar, N.V. Vighnesam, H.S. Takhar, Hall and ion-slip effects in the MHD Couette flow with heat transfer, IEEE Trans. Plasma Sci. 7 (1979) 178–182.
[17] P.C. Ram, H.S. Takhar, MHD free convection from an infinite vertical plate in a rotating fluid with Hall and ionslip currents, Fluid Dyn. Res. 11 (1993) 99–105.
[18] P.C. Ram, A. Singh, H.S. Takhar, Effects of Hall and ionslip currents on convective flow in a rotating fluid with a wall temperature oscillation, J. Magnetohydrodyn. Plasma Res. 5 (1995) 1–16.
[19] H.S. Takhar, B.K. Jha, Effects of Hall and ion-slip currents on MHD flow past an impulsively started plate in a rotating system, J. Magnetohydrodyn. Plasma Res. 8 (1998) 61–72.
[20] O. Anwar Beg, S. Abdul Gaffar, V. Ramachandra Prasad, M.J. Uddin, Computational solutions for non-isothermal, nonlinear magneto-convection in porous media with Hall/ion-slip currents and ohmic dissipation, Eng. Sci. Technol., Int. J. (2015), http://dx.doi.org/10.1016/j.jestch.2015.08.009.
[21] M.A. Mansour, R.S.R. Gorla, Joule heating effects on unsteady natural convection from a heated vertical plate in a micropolar fluid, Can. J. Phys. 76 (12) (1998) 977–984.
[22] O. Anwar Bég, Computational Fluid Dynamic (Spectral DTM) Simulation of Hartmann Flow with Joule Heating: Applications in Liquid Metal Processing, Technical Report, GORT Engovation-Aerospace Research, Bradford, November, UK, 2012.
[23] W.A. Aissa, A.A. Mohammadein, Joule heating effects on a micropolar fluid pasta stretching sheet with variable electric conductivity, J. Comput. Appl. Mech. 6 (1) (2005) 3–13.
[24] S.K. Ghosh, O. Anwar Bég, A. Aziz, A mathematical model for magnetohydrodynamic convection flow in a rotating horizontal channel with inclined magnetic field, magnetic induction and Hall current effects, World J. Mech. 1 (3) (2011) 137–154.
[25] H.M. Duwairi, Viscous and Joule heating effects on forced convection flow from radiate isothermal porous surfaces, Int. J. Numer. Methods Heat Fluid Flow 15 (5) (2005) 429–440.
[26] J. Zueco, O. Anwar Bég, L.M. Lopez-Ochoa, Non-linear transient hydromagnetic partially ionised dissipative Couette flow in a non-Darcian porous medium channel with Hall, ionslip and Joule heating effects, Prog. Comput. Fluid Dyn. 11 (2) (2011) 116–129.
[27] B. Gebhart, J. Mollendorf, Viscous dissipation in external natural convection flows, J. Fluid Mech. 38 (1969) 97.
[28] V.M. Soundalgekar, I. Pop, Viscous dissipation effects on unsteady free convective flow past an infinite vertical porous plate with variable suction, Int. J. Heat Mass Transfer 17 (1) (1974) 85–92.
[29] V. Javeri, Combined influence of Hall effect, ion slip, viscous dissipation and Joule heating on MHD heat transfer in a channel, Heat Mass Transfer 8 (3) (1975) 193–303.
[30] H.S. Takhar, V.M. Soundalgekar, Dissipation effects on MHD free convection flow past a semi-infinite vertical plate, Appl. Sci. Res. 36 (1980) 163–171.
[31] D.L. Turcotte, D.A. Spence, H.H. Bau, Multiple solutions for natural convective flows in an internally heated, vertical channel with viscous dissipation and pressure work, Int. J. Heat Mass Transfer 25 (5) (1982) 699–706.
[32] T. Basu, D.N. Roy, Laminar heat transfer in a tube with viscous dissipation, Int. J. Heat Mass Transfer 28 (3) (1985) 699–701.
[33] A. Barletta, Laminar mixed convection with viscous dissipation in a vertical channel, Int. J. Heat Mass Transfer 41 (22) (1998) 3501–3513.
[34] A. Barletta, E. Rossi di Schio, Effect of viscous dissipation on mixed convection heat transfer in a vertical tube with uniform wall heat flux, Heat Mass Transfer J. 38 (1) (2001) 129–140.
[35] K.S. Chen, J.R. Ho, Effects of flow inertia on vertical, natural convection in saturated porous media, Int. J. Heat Mass Transfer 29 (5) (1986) 753–759.
[36] D.M. Manole, J.L. Lage, The inertia effect on natural convection within a fluid saturated porous medium, Int. J. Heat Fluid Flow 14 (1993) 376–384.
[37] R.E. Powell, H. Eyring, Mechanism for relaxation theory of viscosity, Nature 154 (1944) 427–428.
[38] J. Zueco, O.A. Bég, Network numerical simulation applied to pulsatile non-Newtonian flow through a channel with couple stress and wall mass effects, Int. J. Appl. Math. Mech. 5 (2009) 1–16.
[39] S. Islam, A. Shah, C.Y. Zhou, I. Ali, Homotopy perturbation analysis of slider bearing with Powell–Eyring fluid, Z. Angew. Math. Phys. 60 (2009) 1178–1193.
[40] M. Patel, M.G. Timol, Numerical treatment of Powell–Eyring fluid flow using method of asymptotic boundary conditions, Appl. Numer. Math. 59 (2009) 2584–2592.
[41] V. Ramachandra Prasad, S. Abdul Gaffar, E. Keshava Reddy, O. Anwar Beg, Computational study of non-Newtonian thermal convection from a vertical porous plate in a non-Darcy porous medium with Biot number effects, J. Porous Media 17 (7) (2014) 601–622.
[42] N.S. Akbar, S. Nadeem, T. Hayat, A.A. Hendi, Simulation of heating scheme and chemical reactions on the peristaltic flow of an Eyring–Powell fluid, Int. J. Numer. Methods Heat Fluid Flow 22 (2012) 764–776.
[43] T. Hayat, Z. Iqbal, M. Qasim, S. Obaidat, Steady flow of an Eyring Powell fluid over a moving surface with convective boundary conditions, Int. J. Heat Mass Transfer 55 (2012) 1817.
[44] M. Yürüsoy, A study of pressure distribution of a slider bearing lubricated with Powell–Eyring fluid, Turk. J. Eng. Environ. Sci. 27 (2003) 299–304.
[45] L. Ai, K. Vafai, An investigation of Stokes' second problem for non-Newtonian fluids, Numer. Heat Transfer, Part A 47 (2005) 955–980.
[46] O. Adesanya, J.A. Gbadeyan, Adomian decomposition approach to steady viscoelastic fluid flow with slip through a planer channel, Int. J. Nonlinear Sci. 9 (2010) 86–94.
[47] S. Abdul Gaffar, V. Ramachandra Prasad, E. Keshava Reddy, Computational study of non-Newtonian Eyring–Powell Fluid from a horizontal circular cylinder with Biot number effects, Int. J. Math. Arch. 6 (9) (2015) 133–146.
[48] O. Anwar Bég, O.D. Makinde, Viscoelastic flow and species transfer in a Darcian high-permeability channel, Petrol. Sci. Eng. 76 (2011) 93–99.
[49] H.B. Keller, Numerical methods in boundary-layer theory, Annu. Rev. Fluid Mech. 10 (1978) 417–433.
[50] S. Abdul Gaffar, V. Ramachandra Prasad, E. Keshava Reddy, O. Anwar Beg, Numerical study of non-Newtonian Jeffrey's fluid from a permeable horizontal isothermal cylinder in non-Darcy porous medium, J. Br. Soc. Mech. Sci. Eng. 37 (6) (2015) 1765–1783.
[51] S. Abdul Gaffar, V. Ramachandra Prasad, E. Keshava Reddy, O. Anwar Beg, Flow and heat transfer of Jeffery's non-Newtonian fluid from a horizontal circular cylinder, AIAA J. Thermophys. Heat Transfer 28 (4) (2014) 764–770.
[52] S. Abdul Gaffar, V. Ramachandra Prasad, E. Keshava Reddy, O. Anwar Beg, Flow and heat transfer of non-Newtonian tangent hyperbolic fluid from an isothermal sphere with partial slip, Arab. J. Sci. Eng. 39 (11) (2014) 8157–8174.
[53] S. Abdul Gaffar, V. Ramachandra Prasad, O. Anwar Beg, Computational analysis of magnetohydrodynamic free convection flow and heat transfer of non-newtonian tangent hyperbolic fluid from a horizontal circular cylinder with partial slip, Int. J. Appl. Comput. Math. (IACM) 1 (4) (2015) 651–675.

[54] M. Narayana, P. Sibanda, S.S. Motsa, P.G. Siddheshwar, On double-diffusive convection and cross diffusion effects on a horizontal wavy surface in a porous medium, Bound. Value Probl. 88 (2012) 1–22.
[55] V.R. Prasad, S. Abdul Gaffar, O. Anwar Beg, Non-similar computational solutions for free convection boundary-layer flow of a Nanofluid from an isothermal sphere in a non-Darcy porous medium, J. Nanofluids 4 (2) (2015) 1–11.
[56] F.M. Ali, R. Nazar, N.M. Arifin, I. Pop, Unsteady shrinking sheet with mass transfer in a rotating fluid, Int. J. Numer. Methods Fluids 66 (2011) 1465–1474.
[57] S. Nakamura, Applied Numerical Methods and Software, Prentice-Hall, New Jersey, USA, 1995.
[58] M.I. Anwar, I. Khan, S. Sharidan, M.Z. Salleh, Conjugate effects of heat and mass transfer of nanofluids over a nonlinear stretching sheet, Int. J. Phys. Sci. 7 (2012) 4081–4092.
[59] R.S.R. Gorla, A. Slaouti, H.S. Takhar, Free convection in micropolar fluids over a uniformly heated vertical plate, Int. J. Numer. Methods Heat Fluid Flow 8 (1998) 504–518.
[60] I. Pop, S. Nakamura, Laminar boundary layer flow of power-law fluids over wavy surfaces, Acta Mech. 115 (1996) 55–65.
[61] O. Anwar Bég, Computational Hemodynamics for Hybrid Heart Pump Devices-Finite Element and Nakamura Difference Simulations, Technical Report, Gort Engovation, HEMO-1-4-13, 128 pages, March 2013.
[62] O. Anwar Bég, T.A. Bég, H.S. Takhar, A. Raptis, Mathematical and numerical modeling of non-Newtonian thermo-hydrodynamic flow in non-Darcy porous media, Int. J. Fluid Mech. Res. 31 (2004) 1–12.
[63] O. Anwar Bég, V.R. Prasad, B. Vasu, Numerical study of mixed bioconvection in porous media saturated with nanofluid containing oxytactic micro-organisms, J. Mech. Med. Biol. 13 (4) (2013), http://dx.doi.org/10.1142/S0219519413500 67.
[64] O. Anwar Bég, J. Zueco, M. Norouzi, M. Davoodi, A.A. Joneidi, Assma F. Elsayed, Network and Nakamura tridiagonal computational simulation of electrically-conducting biopolymer micro-morphic transport phenomena, Comput. Biol. Med. 44 (2014) 44–56.
[65] O. Anwar Bég, J. Zueco, S.K. Ghosh, Unsteady hydromagnetic natural convection of a short-memory viscoelastic fluid in a non-Darcian regime: network simulation, Chem. Eng. Commun. 198 (2010) 172–190.